Steady Flow and its Instability of Gravitational Granular Flow

Namiko Mitarai

Department of Chemistry and Physics of Condensed Matter,

Graduate School of Science, Kyushu University, Japan.

A thesis submitted for the degree of Doctor of Science

Kyushu University

January 2003

Abstract

Granular matter consists of a large number of macroscopic particles; the thermal noise has no effect on the particle motion and the interactions are dissipative. These features make the granular flow very different from molecular fluids.

One of the simplest situations to see the complex behavior of granular flow is the gravitational granular flow on a slope. When the inclination angle is small enough, the material stays at rest. The material begins to flow beyond a critical angle; the interaction between the particles is dominated by sustained contacts in the dense and slow flow for the small inclination angle, while the low-density rapid flow is realized for the large enough inclination, where the interaction is dominated by inelastic collisions. Understanding these flowing behaviors is a challenging problem of non-equilibrium statistical physics, not to mention its technological importance. In this thesis, we investigate the fundamental properties of gravitational granular flow. We study the steady flow and its instability by molecular dynamics simulations, and analyze the steady flow by a hydrodynamic model.

Firstly, we clarify the difference between the low-density collisional flow and the dense frictional flow. In the molecular dynamics simulation of the granular material, the soft sphere model with elastic force and dissipation is often used. We examine how the dynamical behavior of steady granular flow changes in the inelastic hard sphere limit of the soft sphere model with keeping the restitution coefficient constant. We find distinctively different limiting behaviors for the two flow regimes, i.e., the collisional flow and the frictional flow. In the collisional flow, the hard sphere limit is straightforward; the number of collisions per particle per unit time converges to a finite value and the total contact time fraction with other particles goes to zero. For the frictional flow, however, we demonstrate that the collision rate diverges as a power of the particle stiffness so that the time fraction of the multiple contacts remains finite even in the hard sphere limit although the contact time fraction for binary collisions tends to zero.

The second subject is to test the applicability of a continuum model to the collisional granular flow in which spinning motion of each grain is considered. In granular material, the angular momentum of the spinning motion is not always negligible because of their macroscopic size. It is known that the mean

spin often deviates from the vorticity of the mean velocity near the boundary. Such a deviation may affect the flow behavior through the coupling of the particle spin and the velocity field. We apply the micropolar fluid model to the collisional flow, which is a continuum model in which the angular velocity field is considered as well as the density and the velocity fields. We demonstrate that, using a simple estimate for the parameters in the theory, the model equations quantitatively reproduce the velocity and the angular velocity profiles obtained from the numerical simulation of the rapid granular flow on a slope.

Finally, we investigate the steady granular flow on a slope and its instability in the low-density regime using the molecular dynamics simulation. We determine the parameter region where the steady collisional flow is realized upon changing the inclination angle and the density of particles. Then we demonstrate that, when the system size is long enough, the collisional granular flow shows clustering instability. It is shown that the uniform flow is less stable for longer system size and/or for lower density.

Contents

Chapter 1

Introduction

1.1 Granular Flow

Granular material consists of particles of macroscopic size [1–3]. The following two important aspects which result from their macroscopic size make the behavior of granular material quite different from conventional molecular systems: (i) the thermal noise plays no role in the motion of grains, and (ii) the interaction between grains is dissipative because of the inelastic collision and the friction. Therefore, we need to supply energy to the system in order to keep granular material in steady motion. Due to these aspects, granular material shows complex behavior which is very different from ordinary solids, liquids, or gases, and has been attracting much interest of physicists in the past decades.

One of the simple examples to see its peculiar behavior is the granular material on a slope under gravity. The grains stay at rest when the inclination angle is small enough. When we gradually increase the inclination angle, an avalanche may occur; parts of the grains flow while other parts may be still at rest. A little more increase of the angle cause the dense, slow flow in which the grains are in contact for large fraction of time. The inelastic collision dominates the interaction when the inclination is large enough. The maximum angle of stability at which the grains start flowing upon increasing the angle from the static state and the angle of repose at which the grains stop flowing upon decreasing the angle are different in general, namely, granular material shows hysteresis. The dynamics of granular flow is a very interesting problem of non-equilibrium statistical physics, besides its technological relevance.

The interactions between grains in flowing granular material are often classified into two types: the impulsive contact (collision) with the momentum exchange and the sustained contact with the transmission of forces [4]. The flow in which the inelastic collision is dominant is called the *collisional flow*, while the flow where the sustained contact dominates is called the *frictional flow*. These two flows show qualitatively different behaviors.

The purpose of our research is to understand the fundamental properties of gravitational granular flow. We choose the granular flow on a slope as a model system because we can see all characteristic behaviors of granular flow. Firstly we clarify the difference between the collisional flow and the frictional flow numerically. After that, we focus on the collisional regime. We examine the applicability of the hydrodynamic description of the steady uniform flow with the spinning motion of each grain, and study the dynamical instability of the uniform flow using the numerical simulation.

1.2 Motivations of Research

1.2.1 Difference between Frictional Flow and Collisional Flow

As for the collisional flow of granular material, its dynamics has some analogy with molecular fluid, and the kinetic theories based on inelastic binary collisions of particles hold to some extent [5–10]. On the other hand, the frictional flow is drastically different from the molecular fluid, and we have little understanding on it. A number of models have been proposed, but the general consensus on the model of dense flow has not been established yet.

For the molecular dynamics simulations of granular material, the following two models have been commonly used, i.e. the inelastic hard sphere model and the soft sphere model.

In the inelastic hard sphere model, the particles are rigid and the collisions are thus instantaneous, therefore its dynamics can be defined through a few parameters that characterize a binary collision because there are no many-body collisions [11]. The model is simple and there are very efficient algorithms to simulate it [12], but it describes basically only the collisional flow because the sustained contact is not allowed. It is also known that the system often encounters what is called the inelastic collapse [2]; the infinite number of collisions take place among a small number of particles in a fi-

nite time, thus the dynamics cannot be continued beyond that point without additional assumption.

On the other hand, in the soft sphere model, which is sometimes called the discrete element method (DEM) in the granular community [11, 13], the particles overlap during collisions and the dynamics is defined through the forces acting on the colliding particles. Collision takes finite time, and not only binary collisions but also many-body collisions and sustained contacts between particles are possible, therefore, both the collisional and the frictional flows may realize in the model. Many researches have been done on granular flow down a slope using DEM [14–19].

In actual simulations, however, the stiffness constants used in the soft sphere model are usually smaller than the one appropriate for real material such as steel or glass ball [20, 21] because of numerical difficulty. Therefore, some part of sustained contact in simulations should be decomposed into binary collisions if stiffer particles are used. It is also not clear that the frictional force in the sustained contact may be described by the same forces with the one suitable for the collisional events.

Therefore, it is important to examine how the system behavior may change as the stiffness constant increases in the soft sphere model, or in other words, how the soft sphere model converges to the inelastic hard sphere model in the infinite stiffness limit. We also expect that the stiffness dependence of the collisional flow and the frictional flow should be qualitatively different. Thus we investigate the system behavior upon changing the stiffness constant systematically with keeping the resulting restitution coefficient constant.

We compare the limiting behaviors of the collisional flow and the frictional flow. It is demonstrated that the interactions between particles in the collisional flow smoothly converge to binary collisions of inelastic hard spheres. In the frictional flow, however, the number of collisions per unit time per particle diverges as a power of the stiffness parameter so that the time fraction of multiple contacts remains finite even in the hard sphere limit although the contact time fraction for binary collisions tends to zero.

1.2.2 Steady Collisional Flow and its Instability

The collisional flow of granular material is described by the inelastic hard sphere model to a degree, thus the kinetic theory based on inelastic binary collisions of particles has been used to analyze it [5–10]. The constitutive equations for hydrodynamic models have been derived based on the kinetic

theory under the assumptions of the slow variation of the variables (the density, the velocity, and the "temperature" which is proportional to the mean square of particle velocity fluctuation) and the molecular chaos.

It is considered that such assumptions can be justified when the system is nearly homogeneous and the density is relatively low. Due to the energy dissipation, the system needs the continuous energy supply to maintain the homogeneous motion without clustering . Such a situation may realize in the flow under strong shear called "rapid granular flow".

The constitutive equations based on the kinetic theory have been tested in the simulations and the experiments of the collisional or rapid granular flow [22–26]. The granular flow on a rough slope with a large inclination is used to investigate the uniform steady behavior of the collisional granular flow experimentally [24, 26].

In most of these hydrodynamic models, the effect of spinning motion of each particle has not been taken into account. In granular flows, however, there is not a great separation between the length scales; the size of each particle is often comparable with the scale of the macroscopic collective motion. Therefore, generally speaking, the angular momentum of the particle spin is not always negligible compared to that of the bulk rotation of mean velocity. Then, the coupling between the rotation of each particle and macroscopic velocity field should have some influence on the flow behavior.

The micropolar fluid model is a continuum model to describe a fluid that consists of particles with spinning motion [27–30]. The model equations include an asymmetric stress tensor and a couple stress tensor; the model can be a suitable framework to describe granular flows.

In this thesis, we apply a micropolar fluid model to the collisional granular flow. We adopt a set of constitutive equations that are a simple and natural extension of those for an ordinary Newtonian fluid. We calculate the velocity and the angular velocity profiles for uniform, steady flow on a slope using the simple estimate of viscosities by elementary kinetic theory. It is demonstrated that the micropolar fluid model reproduces the results of numerical simulations quantitatively, especially the difference between the angular velocity and the vorticity of mean velocity.

In the research on the rheology of granular flow, the uniform steady flow is often considered. It is known, however, that the uniform granular flow often becomes unstable; in the case of the granular flow in a vertical pipe, the instability causes the density wave formation [31, 32]. It is natural to expect that this tendency will cause some instability in the uniform flow on

a slope. Nevertheless, the research on the stability was not so many.

We thus examine the stability of the low-density collisional granular flow on a slope by molecular dynamics simulations. We determine the parameter region where the steady collisional flow is realized upon changing the density of flowing particles and the inclination angle for a particular system size. Then we demonstrate that the collisional granular flow shows clustering instability when the length of the slope is long enough. It is shown that the steady uniform flow is less stable for longer system size and/or for lower density.

1.3 Organization of This Thesis

This thesis is organized as follows. In Chapter 2, we review the research on the gravitational granular flows. The simulation models of granular dynamics, the soft sphere model and the inelastic hard sphere model, are introduced in Chapter 3. In Chapter 4, the stiffness dependence of the granular flow is investigated numerically by taking the hard sphere limit of the soft sphere model. We show that the collisional flow and the frictional flow behave quite differently in the limit. In Chapter 5, the micropolar fluid model is applied to the steady collisional granular flow. It is demonstrated that the model can reproduce the angular velocity profile obtained in the simulation quantitatively. We investigate the instability of the collisional flow by the numerical simulation in Chapter 6. It is shown that the uniform flow shows clustering instability when the length of the slope is large enough and/or the density is sufficiently low. The concluding remarks are given in Chapter 7.

Chapter 2

Gravitational Granular Flow

In this chapter, we briefly summarize the researches on gravitational granular flow and some related topics.

In Section 2.1, we review the motion of a single particle on a bumpy slope, which is the simplest situation that one can think of. Then we outline the researches on the low-density collisional flow and the hydrodynamic models based on the kinetic theory in Section 2.2. In Section 2.3, the researches related to the dense frictional flow are referred.

2.1 Steady Motion of a Single Particle

The motion of a single particle on a bumpy slope has been studied in detail [33–37] to investigate how grains interact with surroundings. In these works, the surface of the slope was made rough by attaching beads of radius r. They controlled the ratio $\Phi = R/r$ of the radius of the moving ball R and r and the inclination angle of the slope θ, and found the following three types of behaviors depending on Φ and θ: (i)The particle stops after a few collisions with the slope for any initial velocity (regime A). (ii)The particle quickly reaches a constant averaged velocity $\bar{v}$ in the direction along the slope and shows almost steady motion (regime B). (iii)The particle jumps and accelerates as it goes down the slope (regime C).

It is interesting that the bifurcation of static and flowing behaviors between the regimes A and B is seen in this very simple situation; this transition reminds us of the angle of repose under which the granular flow stops. Recently, this transition was investigated in detail in connection with the mechanism of the angle of repose in granular pile [38].

One of the motivations of these researches was to obtain some insights about the effective friction force that the flowing grain feels [37, 39, 40]. Following the simple idea originally presented by Bagnold [41], who is one of the pioneers of granular physics, the effective friction force will be proportional to $\bar{v}^2$. The argument is as follows: the momentum loss in each collision with the floor is proportional to $\bar{v}$ on average, and the number of collisions with the bumpy slope per unit time is proportional to $\bar{v}$, thus the momentum loss per unit time should be proportional to $\bar{v}^2$.

The behavior in the regime B has been investigated carefully, and it has been found that the average velocity $\bar{v}$ obeys the form [35]

$$\frac{\bar{v}}{\sqrt{rg}} \propto \Phi^{\beta} \sin\theta, \tag{2.1}$$

in the experiment on the two dimensional inclined plane. This relation means that the effective friction is proportional to $\bar{v}$; if the friction is proportional to $\bar{v}^2$, then $\bar{v}$ should be proportional to $\sqrt{\sin\theta}$. This deviation from the Bagnold's idea has been discussed in terms of the effect of the geometry of the surface [39] and the transverse fluctuation [40]. This is an example that a single particle behavior is already complicated.

The situation in the many-particle system is different from the single particle case. If we discharge a number of balls on the slope with the inclination in the regime B, all of them will finally stop because the average energy in this regime is too small to continue to move after the collision with other particles. Namely, the steady granular flow should appear out of the regime C when we increase the number of the flowing particles. It will be informative for the understanding of the many-body effect in the low-density granular flow to investigate how the single particle picture is modified upon increasing the number of flowing particles.

2.2 Collisional Flow and Hydrodynamic Models

If the flow is dilute and highly sheared, the interaction between grains should be approximated by the inelastic binary collisions. For such a situation, the constitutive equations have been derived by the kinetic theory for slightly inelastic hard spheres [5–10], being inspired by the kinetic theory of dense gas [42]. When the effect of the rotation of each grain is negligible, the

equations for the number density n, the mean velocity $\boldsymbol{u}$, and the granular temperature T are given by

$$\left(\frac{\partial}{\partial t} + \boldsymbol{u}\cdot\nabla\right) n = -n\nabla\cdot\boldsymbol{u}, \tag{2.2}$$

$$mn\left(\frac{\partial}{\partial t} + \boldsymbol{u}\cdot\nabla\right)\boldsymbol{u} = mn\boldsymbol{f} + \nabla\cdot S, \tag{2.3}$$

$$\frac{d}{2}n\left(\frac{\partial}{\partial t} + \boldsymbol{u}\cdot\nabla\right) T = -\nabla\cdot\boldsymbol{q} + S\cdot\nabla\boldsymbol{u} - \Gamma, \tag{2.4}$$

where T is defined as

$$T \equiv \frac{m}{d} < \delta\boldsymbol{u}^2 >, \tag{2.5}$$

with the velocity fluctuation $\delta\boldsymbol{u}$ and the dimension d; $< \ldots >$ means the average. Here, $\boldsymbol{f}$ is the external force per unit mass, and S and $\boldsymbol{q}$ are the stress and the heat flux, respectively. The constitutive equations have been derived up to the first order of spatial gradient (the Navier-Stokes order) [6–8] and the second order (the Burnett order) [9]. The smallness of the inelasticity as well as the smallness of the spatial gradient is assumed in the calculation, therefore the quantitative agreement with experiments and simulations is expected to be limited.

What makes this granular fluid distinctively different from the molecular fluid is the energy dissipation term in Eq. (2.4), Γ, which appears due to the inelasticity of collisions. If no energy is supplied to the system, the temperature decays and the relative motion between particles becomes very small. In the case of the free cooling inelastic hard sphere system, this causes instabilities in the homogeneous state and leads to the the development of vortex structure in the velocity field, the clustering, and eventually the inelastic collapse in a finite time [8, 43–46].

When we inject large enough energy to the system continuously, the collisional regime may be maintained and then the hydrodynamic model should work to some extent. It has been shown that the model can reasonably reproduce the results of the simulations and the experiments of the steady flow under strong shear [22, 23] or the steady flow on a inclined plane [24–26]; recently the shock propagation in vertically oscillated granular layers is successfully reproduced by the Navier-Stokes model [47]. The practical efficiency of this type of models for the rapid collisional flows is now accepted in the granular community.

The validity of a continuum description of granular materials, however, has been questioned and remains as an open problem [2]. Even in the rapid collisional flow, the Navier-Stokes model fails to describe the flow behavior at very close to the boundary [26]. One of the reasons of this deviation should be the spinning motion of each grain. It has been known that the mean spin often deviates from the vorticity of the mean velocity near the boundary [32, 48]. In addition, the angular momentum of the spinning motion is not always negligible compared to that of the rotation of bulk velocity, because of the macroscopic size of the particles. When we consider the grains with rough surface or of arbitrarily shapes, it is possible that the coupling between the particle spin and the mean velocity has some influence on the macroscopic flow behavior.

The micropolar fluid model is a continuum model to describe a fluid that consists of particles with spinning motion [27–30]. The angular velocity field as well as the density and the velocity fields is considered in the model equations, and an asymmetric stress tensor and a couple stress tensor are included. Therefore, the model can be a suitable framework to describe granular flows.

Some researches have been carried out to incorporate the spin into the kinetic theory for granular materials to obtain the constitutive equations with the effect of particle spin [49–51]. However, the effect of the couple stress was neglected in most of them; when they solved the obtained hydrodynamic equations, it has been assumed that the mean spin matches with the vorticity of the mean velocity, and the deviation near the boundary was not considered.

In the meantime, the micropolar fluid model has been applied to dense granular flows [52, 53]. However, the constitutive equations adopted for the stress and the couple stress tensors were very complicated; it was difficult to interpret the results physically. The application of the micropolar fluid model with simple constitutive equations to the collisional flow will help us to understand the effect of the particle spin in granular flow.

Another interesting issue on granular flow is its dynamical instability. In most of the researches on rheology of collisional granular flow, the steady uniform flow is considered. It is known, however, that uniform granular flow often shows instabilities owing to the energy dissipation. The granular flow on a slope often exhibits the coexistence of the collisional regime and the frictional regime [4, 14, 54]. In the case of the shear flow of inelastic particles, the formation of microstructure or small clusters has been observed numerically [55]. The instability cause the density wave formation in the

granular flow in a vertical pipe where the power spectrum of the density fluctuation obeys a power law [31, 56–60]. Recently, the wave formation of granular flow on a slope has been found experimentally in rather low-density flow [61] and in the dense flow [62]. It is important to investigate the dynamical instability in rapid granular flow because the formation of dense region may imply the breakdown of the collisional behavior.

2.3 Frictional Flow

When the injection of energy to the system is small, sustained contacts and many-body collisions take place and the kinetic theory based on binary collisions fails. Such a slow, dense, and frictional flow is widely found in real systems under gravity.

One of the examples of the frictional flow found in our daily life is the flow on the surface of a granular pile. When we observe the cross-section of the surface flow, it is found that only thin layer of granular material is flowing rapidly, and the width of the layer is the order of 10 diameters of grains [1]. Komatsu *et al.* have shown in their experiment of steady flow on a granular pile that the grains in the "frozen" bulk region, namely, the grains below the rapidly flowing layer, exhibit creeping motion with the velocity profile decaying exponentially [63]. The surface flow of granular material in a rotating drum has been also investigated [64, 65]. In these surface flows, the angle of the flowing surface is close to the angle of repose and the rapidly flowing layer is thin; the angle and the depth of the flowing layer is determined spontaneously.

For the flow on a solid plane, in contrast, both the inclination angle and the flow depth can be controlled. In this geometry, the flow behavior strongly depends on the roughness of the solid plane. When the flat bottom is used, the high shear rate region is confined in the thin layer near the bottom, and the bulk of material over that sheared layer slides down with very small shear rate [62, 66]. In the case of rough bottom, the slip velocity at the boundary becomes smaller, while the velocity profile depends very much on the height of the flowing material and the inclination angle [67].

The cause of the complex behavior is the various types of interactions in the dense granular flow; we should consider not only the inelastic collisions but also the static and the dynamical friction force, and the effect of arching or force chain. The excluded volume effect also plays an important role. At

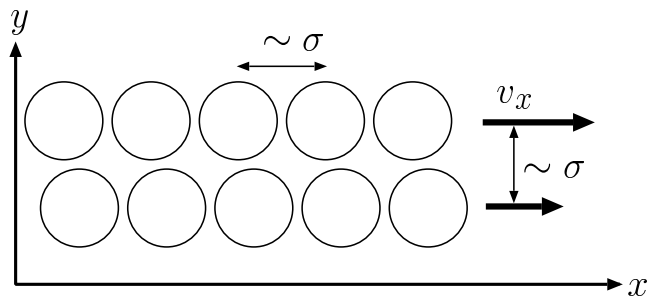

Figure 2.1: Schematic illustration of the situation considered by Bagnold.

this moment, we know little about each interactions, and needless to say, the effect of each interaction on the flow behavior. It is necessary to investigate more about the fundamental properties of the dense flows.

The modeling of the dense flow is very difficult because of this situation, and a general consensus on the model of the dense frictional flow does not exist. We present the outlines of some of the models, but it is impossible to list all of them.

Considering the situation where the role of the collisional and the frictional interactions are comparable [4], it has been tried to include the effect of frictional force in the constitutive relation for the rapid granular flows [62, 68]. Some recent works on dense gravity flow consider the non-local transmission of forces because of the network of contacting grains [69, 70]. The more phenomenological continuum model called the depth-averaged (Saint-Vernert) equations [71–73] use the experimentally observed velocity profile to determine the force in the flow, and succeeded to reproduce some experimentally observed phenomena in the surface flow or the avalanche.

Let us introduce a famous argument about the stress-strain relation of the dense flow before concluding this section. It is called the *Bagnold's law* [41], which gives the shear stress proportional to the square of the strain rate.

Consider grains with mass m and diameter σ flowing in the x direction [74]. When the flow is dense and the grains form "layers" in the y direction (Fig. 2.1), the difference of the velocity between layers is given by $\sigma\partial_y v_x(y)$, where $v_x(y)$ is the flow velocity at the height y and ∂_y is the partial derivative with respect to y. Then the order of the momentum transfer per one collision between particles at different heights is estimated as $\Delta p \sim m\sigma\partial_y v_x$, while the collision per unit time, n_c, is estimated by $n_c \sim \sigma(\partial_y v_x)/\sigma = (\partial_y v_x)$.

Therefore, the shear stress, S_{yx}, is estimated as

$$S_{yx} \sim \frac{1}{\sigma^2}\Delta p n_c \sim \frac{m}{\sigma}(\partial_y v_x)^2, \tag{2.6}$$

which is the famous Bagnold's law.

This law gives a simple scaling law between the total height of the flow h and the flow velocity v_x when it is applied to the steady flow on an inclined plane with the inclination angle θ. The equation of motion in the x direction is given by $\rho(y)g\sin\theta + \partial_y S_{yx} = 0$, where ρ is the mass density and g is the acceleration of gravity. When the density is high and thus ρ can be considered as a constant over the flow depth, it gives

$$S_{yx} = \rho g(h-y)\sin\theta, \tag{2.7}$$

where h is the depth of the flowing material. From Eqs. (2.6) and (2.7), we get

$$v_x(y) = A[h^{3/2} - (h-y)^{3/2}] \tag{2.8}$$

when $v_x(0) = 0$, with a constant A. Finally we obtain the scaling law

$$v_x(h) = Ah^{3/2}. \tag{2.9}$$

A recent experiment on the dense flow down a rough slope performed by Pouliquen revealed a simple scaling law of velocity [75]. He changed the height of the flowing grains h and the inclination angle θ, and measured the flow velocity u. He determined the line $h = h_{stop}(\theta)$ in the θ vs. h plane, below which the flow stops. This indicates the angle of repose depends on the height of the flowing layer. Then he found that the flow velocity of different θ or different material obeys the scaling law

$$\frac{u}{\sqrt{gh}} = \beta\frac{h}{h_{stop}(\theta)}, \tag{2.10}$$

with the acceleration of gravity g and a numerical constant β. This law can be regarded as an extension of Eq. (2.9). Such a simple scaling is surprising for those who are studying the physics of the dense granular flow, and is the active topic of current study [67, 76, 77].

Chapter 3

Modeling of Interactions in Granular Material

As emphasized in Chapter 1 and 2, the dissipative nature of the interactions between gains makes them behave very differently from molecular systems. Some simple phenomenological models with dissipative interactions have succeeded to reproduce the characteristic behaviors of granular material, though the detail of interactions between grains such as the friction and the plastic deformation are very complicated and still under discussion [11]. In this chapter, we introduce two models which have been commonly used for the simulations of granular dynamics; they are the soft sphere model called the discrete element method (DEM) and the inelastic hard sphere model. The correspondence of parameters between the two models is discussed in the last section.

3.1 Discrete Element Method (DEM)

In the soft sphere model, which is sometimes called the discrete element method (DEM) in the granular community [11, 13, 78], the particles overlap during collision and the dynamics is defined through the forces acting on the colliding particles. Collision takes finite time, thus not only the binary collision but also the many-body collision and the sustained contact between particles are possible; both the collisional and the frictional flows may realize in the model. It is widely used for molecular dynamics simulations of granular flow on a slope under gravity [14–19].

Here we introduce the two dimensional model with the linear elastic force

and dissipation. The extensions of the model to three dimension or to the non-linear force law are found in Refs. [11, 78].

Let us consider the two disks i and j of the diameters σ_i and σ_j and the masses m_i and m_j at the positions $\boldsymbol{r}_i$ and $\boldsymbol{r}_j$ with the velocities $\boldsymbol{c}_i$ and $\boldsymbol{c}_j$ and the angular velocities $\boldsymbol{\omega}_i$ and $\boldsymbol{\omega}_j$. If the particles are in contact, namely,

$$\Delta \equiv \frac{\sigma_i + \sigma_j}{2} - |\boldsymbol{r}_{ij}| > 0, \tag{3.1}$$

where $\boldsymbol{r}_{ij} \equiv \boldsymbol{r}_i - \boldsymbol{r}_j$, the force acting on the particle i from the particle j is calculated as follows: The relative velocity of the point of contact $\boldsymbol{v}_{ij}$ is given by

$$\boldsymbol{v}_{ij} = (\boldsymbol{c}_i - \boldsymbol{c}_j) + \boldsymbol{n} \times \left(\frac{\sigma_i}{2}\boldsymbol{\omega}_i + \frac{\sigma_j}{2}\boldsymbol{\omega}_j \right), \tag{3.2}$$

with the normal vector $\boldsymbol{n} = \boldsymbol{r}_{ij}/|\boldsymbol{r}_{ij}| = (n_x, n_y, 0)$. Then the normal velocity v_n, the tangential velocity v_t, and the tangential displacement u_t at the contact point are given by

$$v_n = \boldsymbol{n} \cdot \boldsymbol{v}_{ij}, \qquad v_t = \boldsymbol{t} \cdot \boldsymbol{v}_{ij}, \tag{3.3}$$

$$u_t = \int_{t_0}^{t} v_t \mathrm{d}t, \tag{3.4}$$

with $\boldsymbol{t} = (-n_y, n_x, 0)$. Here, t_0 is the time when the two particles start to be in contact. Then the normal force F_n^{ij} and the tangential force F_t^{ij} acting on the particle i from the particle j are given by

$$F_n^{ij} = 2Mk_n\Delta - 2M\eta_n v_n, \tag{3.5}$$

$$F_t^{ij} = \min(|h_t^{ij}|, \mu|F_n^{ij}|)\mathrm{sign}(h_t^{ij}) \tag{3.6}$$

with

$$h_t^{ij} = -2Mk_t u_t - 2M\eta_t v_t, \tag{3.7}$$

where k_n and k_t are elastic constants, η_n and η_t are damping parameters, and $M = m_i m_j/(m_i + m_j)$ is the reduced mass [1]. μ is the Coulomb friction coefficient for sliding. No force is applied between the particles i and j when $\Delta < 0$. In the simulations, the equation of motion of each particle is numerically integrated with a certain time step.

This phenomenological model simply expresses the normal and tangential elastic force by linear springs, the dissipations by linear dashpots, and the

[1] The reason why we introduced the reduced mass here is to simplify the expressions of the correspondence of the DEM parameters to the parameters in the inelastic hard sphere model. (See Section 3.3.)

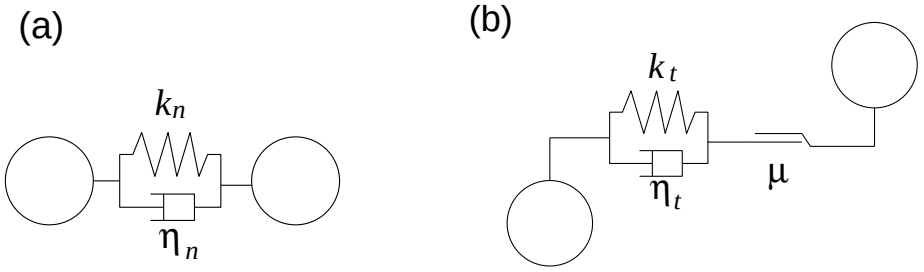

Figure 3.1: A schematic illustration of the interactions in DEM. The normal interaction (a) is expressed by a linear spring and a dashpot, and the tangential interaction (b) is expressed by a linear spring, a dashpot, and a slider.

friction force by a slider, as illustrated in Fig. 3.1. Although this force law is simplified very much from the real interaction in granular material, the disadvantage of this model is that it still contains many parameters; it is difficult to determine all the parameters from the material parameters obtained experimentally [79]. The way to determine the DEM parameters has not been established yet, but the experience shows that observed phenomena are often not so sensitive to the detail of parameters; this allows DEM to reproduce many experiments from static to dynamic behaviors [21, 78].

3.2 Inelastic Hard Sphere Model

In the inelastic hard sphere model, the particles are infinitely rigid. The collisions are instantaneous and there is no many-body collision, which allows us to define its dynamics through a few parameters that characterize a binary collision [11]. We summarize the collision rule in terms of the normal and tangential restitution coefficients and the sliding friction [80]. The rule is constructed so that the energy is dissipated but the momentum is conserved through the collision.

Let us consider a collision between the two spheres i and j at the contact positions $\boldsymbol{r}_i$ and $\boldsymbol{r}_j$, respectively. Prior to the collision, they have the velocities $\boldsymbol{c}_i$ and $\boldsymbol{c}_j$ and the angular velocities $\boldsymbol{\omega}_i$ and $\boldsymbol{\omega}_j$. Then the relative velocity of the point of contact $\boldsymbol{v}_{ij}$ is given by

$$\boldsymbol{v}_{ij} = (\boldsymbol{c}_i - \boldsymbol{c}_j) + \boldsymbol{n} \times \left(\frac{\sigma_i}{2}\boldsymbol{\omega}_i + \frac{\sigma_j}{2}\boldsymbol{\omega}_j \right), \tag{3.8}$$

where the normal vector $\boldsymbol{n} = \boldsymbol{r}_{ij}/|\boldsymbol{r}_{ij}|$ with $\boldsymbol{r}_{ij} = \boldsymbol{r}_i - \boldsymbol{r}_j$.

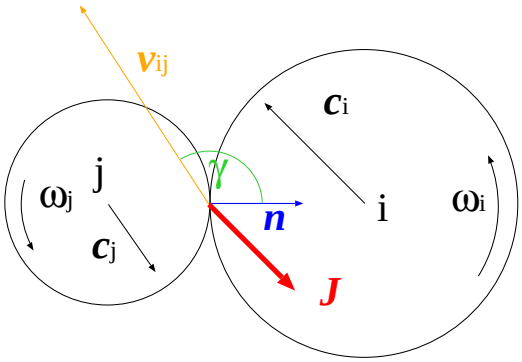

Figure 3.2: The collision of inelastic hard spheres.

If $\boldsymbol{v}'_{ij}$ denotes the relative velocity after the collision, the collision rule for normal direction is

$$(\boldsymbol{n} \cdot \boldsymbol{v}'_{ij}) = -e_n(\boldsymbol{n} \cdot \boldsymbol{v}_{ij}), \tag{3.9}$$

where e_n is the normal restitution coefficient with $0 \leq e_n \leq 1$; $e_n < 1$ leads to the inelastic collision where kinetic energy is dissipated.

For the collision law in the tangential direction, we consider the sliding of particles at the contact point with the Coulomb friction force. It gives

$$|\boldsymbol{n} \times \boldsymbol{J}| = \mu(\boldsymbol{n} \cdot \boldsymbol{J}), \tag{3.10}$$

with the Coulomb friction coefficient μ, where $\boldsymbol{J}$ is the momentum change of the particle i through the collision. It is easy to show that Eqs. (3.9) and (3.10) gives

$$\boldsymbol{J} = M(1 + e_n)[\mu \boldsymbol{v}^t_{ij} \cot\gamma - \boldsymbol{v}^n_{ij}], \tag{3.11}$$

where $\boldsymbol{v}^n_{ij} = (\boldsymbol{n} \cdot \boldsymbol{v}_{ij})\boldsymbol{n}$ and $\boldsymbol{v}^t_{ij} = \boldsymbol{v}_{ij} - \boldsymbol{v}^n_{ij}$. Here, γ is the angle between $\boldsymbol{n}$ and $\boldsymbol{v}_{ij}$, defined so that $\pi/2 \leq \gamma \leq \pi$ (Fig. 3.2).

This relation (3.11) shows that $\boldsymbol{J}$ diverges when $\gamma \to \pi$. In order to improve this model so that it can be applied to the central collision with $\gamma \to \pi$, we introduce another parameter;

$$(\boldsymbol{n} \times \boldsymbol{v}'_{ij}) = -\beta(\boldsymbol{n} \times \boldsymbol{v}_{ij}), \tag{3.12}$$

where β is the tangential restitution coefficient with $-1 \leq \beta \leq 1$. Under Eq. (3.12), the momentum change $\boldsymbol{J}'$ is given by

$$\boldsymbol{J}' = -M(1 + e_n)\boldsymbol{v}^n_{ij} - M'(1 + \beta)\boldsymbol{v}^t_{ij}, \tag{3.13}$$

with

$$\frac{1}{M'} = \frac{1}{M} + \frac{1}{4}\left(\frac{\sigma_i^2}{I_i} + \frac{\sigma_j^2}{I_j}\right), \tag{3.14}$$

where I_i is the moment of inertia of the particle i. For the two dimensional disks with $I_i = m_i\sigma_i^2/8$, it gives $M' = M/3$.

The collision rule in the tangential direction depends on γ. The critical value, γ_0, which determine whether particles slide or not, is given by $\boldsymbol{J} = \boldsymbol{J}'$, namely,

$$\tan\gamma_0 = -\mu\frac{M(1+e_n)}{M'(1+\beta)}. \tag{3.15}$$

Equation (3.10) is applied when $\gamma < \gamma_0$, and Eq. (3.12) is applied when $\gamma > \gamma_0$.

The collision of perfectly smooth particles corresponds to $\beta = -1$ and $\mu = 0$, because $\boldsymbol{v}_{ij}^t$ does not change through the collision in this case. Such a simple model with $e_n < 1$, namely, the model in which the energy dissipates through the inelastic normal collision only, have been widely used to investigate the fundamental properties of granular system [2, 43, 44, 46, 81, 82]. The rule without the Coulomb friction which is characterized by e_n and β only is also often used as a simple model with the particle rotation [8, 49, 51].

Because the collisions are instantaneous, the event-driven method is used for numerical simulation of the inelastic hard sphere system. Very effective algorithms have been developed for the event-driven simulation of hard sphere systems [12], which enables to simulate very large system.

The problem of the inelastic hard sphere model is that it cannot be used for the situation where the sustained contact occurs. It is known that the system often shows the singular behavior which is called *inelastic collapse*, namely, the infinite number of collision among a small number of particle within a finite time [2] [2] ; the dynamics cannot go beyond this point without additional assumption. Therefore, the situations where the inelastic hard sphere model is applicable are rather limited.

3.3 Correspondence of Parameters between the Models

One of the advantages of the inelastic hard sphere model to DEM is its simplicity; parameters in the former is fewer than those in the latter. When

[2]The more description of the inelastic collapse is given in Section 4.2.

we adopt the linear dependence of the elastic and viscous force on the overlap Δ and the relative velocity, respectively, we can relate the parameters in DEM to those in the inelastic hard sphere model [83]. In the following, we briefly summarize the correspondence of the parameters.

Suppose that the particle i at $\boldsymbol{r}_i(t) = (x_i(t), 0)$ and the particle j at $\boldsymbol{r}_j(t) = (x_j(t), 0)$ collide at $t = 0$ with the relative velocity $\dot{\boldsymbol{r}}_j(0) - \dot{\boldsymbol{r}}_i(0) = (-v_0, 0)$, where the dots represent the time derivatives. The overlap of the two particles is $\Delta(t) = (\sigma_i+\sigma_j)/2-(x_i(t)-x_j(t))$ and the equation of motion for $\Delta(t)$ becomes

$$\begin{aligned} \ddot{\Delta} &= \ddot{x}_j - \ddot{x}_i \\ &= -2\eta_n\dot{\Delta} - 2k_n\Delta, \end{aligned} \tag{3.16}$$

from Eq. (3.5). With the initial conditions $\Delta(0) = 0$ and $\dot{\Delta}(0) = v_0 > 0$, we get

$$\Delta(t) = \frac{v_0}{\sqrt{2k_n - \eta_n^2}} \exp\left(-\eta_n t\right) \sin\left(\sqrt{2k_n - \eta_n^2}t\right). \tag{3.17}$$

The collision ends when $\Delta(t) = 0$, thus the duration of the contact τ_c and and the normal restitution coefficient e_n are given by

$$\tau_c = \frac{\pi}{\sqrt{2k_n - \eta_n^2}} \tag{3.18}$$

and

$$e_n = \exp\left(-\frac{\pi\eta_n}{\sqrt{2k_n - \eta_n^2}}\right), \tag{3.19}$$

respectively. [3]

The similar relations can be obtained for the binary collision with non-zero tangential relative velocity. Neglecting the Coulomb friction and $\dot{\boldsymbol{n}}$ during the contact, [4] the equation for the tangential displacement $u_t(t)$ is written in the following form [83];

$$\ddot{u}_t = -(2k_t u_t + 2\eta_t \dot{u}_t)\frac{M}{M'} \tag{3.20}$$

[3] This relation holds for the normal collision only; otherwise we need to take into account the variation of the normal vector $\boldsymbol{n}$ for the calculation of $\Delta(t)$. In the hard sphere limit of $k_n \to \infty$ (see Section 4.1), however, we can neglect the variation $\boldsymbol{n}$ during the collision, and the expression (3.19) corresponds to e_n in the hard sphere model.

[4] The variation of $\boldsymbol{n}$ during the collision becomes negligible in the hard sphere limit, as denoted above.

where M' is given in Eq. (3.14). Therefore, a half period of the tangential oscillation is given by

$$\tau_s = \frac{\pi}{\sqrt{6k_t - 9\eta_t^2}} \tag{3.21}$$

for two dimensional disks with moment of inertia $I_i = m_i\sigma_i^2/8$. Here we choose the parameters k_t and η_t so that the relation $\tau_s = \tau_c$ is satisfied:

$$\sqrt{6k_t - 9\eta_t^2} = \sqrt{2k_n - \eta_n^2}. \tag{3.22}$$

Under this condition, the tangential restitution coefficient is given by

$$\beta = \exp(-3\eta_t\tau_c). \tag{3.23}$$

Now we have the expressions of all the parameters in the collision rule of the inelastic hard sphere model: e_n, β, and μ. When the parameters are chosen so that these relations hold, the only additional parameter in DEM is k_n, which determines the duration of contact τ_c.

Though it is known that the restitution coefficients are not simple constants in real material and depends on the relative velocity and the collision angle [84, 85], they are often given in the literature of the experiments of granular material. One possible way to determine the DEM parameters may be to use these relations to obtain the desired restitution coefficients. It should be questioned, however, whether the force suitable for the collisional events describes the frictional force in the sustained contact properly.

How can we determine the duration of contact τ_c? In general τ_c depends on the detail of the collision, but the order of τ_c may be estimated by the theory of elasticity. The elastic energy U_e stored by two identical three-dimensional spheres deformed over the depth Δ is derived by Hertz [11, 86], which is given by

$$U_e = \frac{1}{2}k\Delta^{5/2}, \tag{3.24}$$

with

$$k = \frac{4}{15}\frac{E}{1-\nu^2}\sqrt{\sigma}, \tag{3.25}$$

where E and ν are Young's modulus and Poisson's coefficient, respectively [5]. Therefore, when the relative velocity of the spheres at the moment of contact is v_0, the energy conservation law reads

$$\frac{1}{2}Mv_0^2 = \frac{1}{2}k\Delta^{5/2} + \frac{1}{2}M\dot{\Delta}^2. \tag{3.26}$$

[5]The Hertz's theory gives the elastic force proportional to $\Delta^{3/2}$. The DEM with the elastic force of this non-linear dependence on Δ is also widely used.

Material	$E[\mathrm{N/m^2}]$	ν	$\rho_p[\mathrm{g/cm^3}]$
Glass	7.13×10^{10}	0.22	$2.2 - 3.6$
Steel	$20.1 \times 10^{10} - 21.6 \times 10^{10}$	$0.28 - 0.3$	7.86

Table 3.1: The material parameters used in the estimation of τ_H, taken from Ref. [87].

Then we obtain the duration of contact τ_H as [11, 86]

$$\tau_H = \frac{4\sqrt{\pi}\Gamma(2/5)}{5\Gamma(9/10)} \left(\frac{M^2}{k^2 v_0}\right)^{1/5} \sim 2.94 \left(\frac{M^2}{k^2 v_0}\right)^{1/5}. \tag{3.27}$$

This gives us $\tau_H \sim 8.4 \times 10^{-6}$ s for the collision of glass or steel beads with $\sigma = 1.5$ mm and $v_0 = 5$ cm/s using E, ν and the mass density ρ_p given in Table 3.1. Whereas the typical time scale of the motion of grains under gravity is estimated by $\tau_0 = \sqrt{\sigma/g}$, which is 1.2×10^{-2} s in this case; thus $\tau_H/\tau_0 \sim 7 \times 10^{-4}$. In the DEM simulation, the time step for the numerical integration is limited by the smaller time scale, namely, the duration of contact. One often use the value of k_n which gives rather large τ_c for the efficiency of the numerical simulation, hopefully expecting that the system behavior is not so sensitive to the value of τ_c if it is small enough compared to the typical time scale of the collective motion.

In this thesis, we adopt DEM as the simulation model. It is suitable for the gravitational flow where both the collisional event and the sustained contact occurs. We investigate the stiffness dependence of the steady granular flow by taking the inelastic hard sphere limit of DEM in Chapter 4.

Chapter 4

Hard Sphere Limit of DEM: Stiffness Dependence of Steady Granular Flows

The granular flows are classified into two types as has been described in Chapter 1 and 2, i.e., the *collisional flow* and the *frictional flow*, depending on the dominant interaction; the former is dominated by the inelastic collision and the latter is dominated by the sustained contact.

For the simulation of granular flow, the models introduced in Chapter 3, the soft sphere model (DEM) and the inelastic hard sphere model, are commonly used.

The inelastic hard sphere model is effective to investigate the fundamental properties of collisional granular flow thanks to its simplicity. However, it cannot be used for the frictional flow, because the sustained contact is not allowed. It is also known that the system often encounters the inelastic collapse.

The both flows may realize in DEM. However, the stiffness parameter used in DEM is often much smaller than the one appropriate for the real materials like steel or glass ball. It is also not clear that the frictional force in the sustained contact may be described by the same forces with the one suitable for the collisional events. Therefore, it is important to examine how the system behavior changes upon increasing the stiffness of particles with keeping the restitution constant unchanged, or taking the inelastic hard sphere limit of DEM.

In this chapter, we numerically investigate how the behavior of the col-

lisional flow and the frictional flow change on taking the hard sphere limit of DEM. In Section 4.1, we summarize how we take the hard sphere limit keeping the restitution coefficient constant; we use the correspondence of parameters given in Section 3.3. Then we discuss the limiting behavior in some simple situations where the hard sphere model results in the inelastic collapse in Section 4.2. In Section 4.3, the simulation results are shown. At first, the stiffness dependence of the steady motion of a single particle rolling down a slope is presented to see how the inelastic collapse appears in the hard sphere limit. Then, the collisional flow and the frictional flow are examined. We find that the interactions between particles in the collisional flow smoothly converge to binary collisions of inelastic hard spheres, while those in frictional flow shows non-trivial behavior; the behavior is also different from the "inelastic collapse" in the single particle system. The summary and the discussion are given in Section 4.4.

4.1 Hard sphere Limit of DEM

We summarize how we take the hard sphere limit using the correspondence of parameters.

The binary collision rule in the inelastic hard sphere model in Section 3.2 is determined by the normal restitution constant e_n (Eq. (3.9)), the tangential restitution constant β (Eq. (3.12)), and the Coulomb friction coefficient μ (Eq. (3.10)). In DEM, the force acting on the colliding particle is determined by the normal stiffness constant k_n and the damping parameter η_n (Eq. (3.5)), the tangential stiffness constant k_t and the damping parameter η_t (Eq. (3.7)), and the Coulomb friction coefficient μ (Eq. (3.6)).

In Section 3.3, the following relations are shown: The duration of contact τ_c for a normal binary collision and the normal restitution coefficient e_n in DEM are given in Eqs. (3.18) and (3.19), respectively. The tangential restitution coefficient β is given by Eq. (3.23) under the condition (3.22).

Equations (3.18) and (3.19) can be rewritten as

$$\eta_n = \left[\frac{2k_n}{(\pi/\ln e_n)^2+1}\right]^{1/2}, \tag{4.1}$$

$$\tau_c = \left[\frac{\pi^2+(\ln e_n)^2}{2k_n}\right]^{1/2}. \tag{4.2}$$

Using these relations, we can take the inelastic hard sphere limit of this model for given restitution coefficients e_n and β by taking the $k_n \to \infty$ limit; η_n,

η_t, and k_t are given by Eqs. (4.1), (3.23), and (3.22), and the duration time of collision τ_c goes to zero as Eq. (4.2).

4.2 Inelastic Collapse

It is well known that the inelastic hard sphere system can undergo *inelastic collapse*, the phenomenon where infinite collisions take place within a finite period of time [2]. A simple example is the vertical bouncing motion of a ball under gravity. When the collision between the floor and the ball is inelastic, the velocity of the ball just before the nth collision v_n and the next one have the relation

$$v_{n+1} = e_w v_n \tag{4.3}$$

with $0 \leq e_w < 1$; the ball undergoes the infinite number of collision within the period $2v_0/[g(1 - e_w)]$.

The inelastic collapse also occurs without gravity. The simplest example is three inelastic balls in one dimension, and a ball goes back and forth between the other two approaching each other; the three balls lose relative velocity completely in the limit of infinite collisions [88, 89]. The inelastic collapse has been also found in the event-driven simulations of free cooling inelastic hard sphere system in higher dimension [90, 91]. Furthermore, it has been recently reported that the inelastic collapse occurs even in the shear flow, although it is natural to think that the shear tends to prevent the collapse [92].

The inelastic collapse never occurs in the soft sphere model. However, it is worth to discuss what will happen in the soft sphere model in a simple situation where the inelastic collapse occurs in the hard sphere model.

Let us consider the vertical bouncing motion of a soft ball under gravity at first. We assume the same force law between the ball and the floor as in Eqs. (3.5) and (3.6), except that we replace $2M$ by the mass of the ball m. When the ball and the floor are in contact, the equation of motion for the overlap of the ball and the floor, z, is given by

$$\ddot{z} + k_n z + \eta_n \dot{z} = g. \tag{4.4}$$

Therefore, when the velocity just before the collision is small enough, the ball cannot take off from the floor, and finally reaches the steady state of keeping contact, $z = g/k_n > 0$. One can show that, if the impact velocity v_i is below a critical value v_c, which is $O(1/\sqrt{k_n})$ for large enough k_n (Appendix B), the

ball stays in contact with the floor; for $v_i \gg v_c$, the restitution coefficient e_w defined in Eq. (4.3) can be considered as a constant. Therefore, for a given initial impact velocity v_0, the number of necessary collisions n_c for the ball to stay in contact with the floor is roughly estimated by the condition $e_w^{n_c} v_0 \sim v_c$, namely, $n_c \sim \log(v_c/v_0) / \log e_w$. Because $v_c \sim 1/\sqrt{k_n}$ for large k_n, n_c behaves as

$$n_c \propto \log k_n + \text{const.} \tag{4.5}$$

in the hard sphere limit. Thus n_c diverges logarithmically when $k_n \to \infty$, which correspond to the inelastic collapse due to gravity.

In the case without gravity, the inelastic collapse results in the "many-body collision" in the soft sphere model. For example, when we consider three soft spheres in one dimension, the binary collision can be approximated by the collision law with a constant restitution coefficient. However, when the interval between two collisions becomes smaller than the duration of contact τ_c, the three balls are in contact at the same time, namely, the three-body collision occurs. They still have some relative motion, thus they will fly apart after that. The number of collisions before the three-body collision will also diverge logarithmically in the hard sphere limit because $\tau_c \propto 1/\sqrt{k_n}$.

One should note that a many-body collision in the soft sphere model does not necessarily result in the inelastic collapse in the hard sphere limit. Actually, in most of the cases, a many-body collision will be decomposed into a set of binary collisions in the hard sphere limit.

4.3 Simulation Results

In this section, we investigate the stiffness dependence of granular material on a slope in the following three situations: (i) a single particle rolling down a slope, (ii) the dilute collisional flow, and (iii) the dense frictional flow. We focus on the steady state in each situation and compare the simulation data with changing k_n systematically. The particles are monodisperse in (ii), while they are polydisperse in (iii) in order to avoid crystallization.

In the simulations, the parameters have been chosen to give $e_n = \beta = 0.7$, $\mu = 0.5$ in the hard sphere limit. Each particle is also subject to the gravity, and the gravitational acceleration is given by $\boldsymbol{g} = g(\sin\theta, -\cos\theta)$. All values are non-dimensionalized by the length unit σ, the mass unit m, and the time unit $\sqrt{\sigma/g}$. Here, σ is the diameter of the largest particle in the system and m is the mass of that particle. The second order Adams-Bashforth method

and the trapezoidal rule are used to integrate the equations for the velocity and the position, respectively [93]. Note that the time step for integration, dt, needs to be adjusted as τ_c becomes smaller. All the data presented in this chapter are results with $dt = \min(\tau_c/100, 10^{-4})$. We have confirmed that the results do not change for $dt \leq \tau_c/100$ by calculating also with $dt = \tau_c/50$ and $dt = \tau_c/200$ in the case of the single particle.

4.3.1 A single particle rolling down a bumpy slope

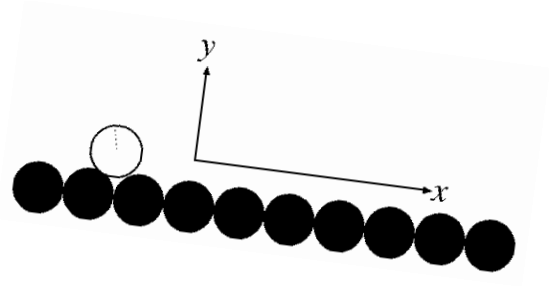

Figure 4.1: A snapshot of a single ball rolling down a rough slope.

Let us first consider a single particle rolling down a bumpy slope which has been referred in Section 2.1. In the simulations, we make the boundary rough by attaching the same particles with the rolling one to the slope with the spacing 0.002σ (see Fig. 4.1). For the chosen parameters with the normal stiffness $k_n = 2^{-1} \times 10^5$, the range of θ for which steady motion is realized is $0.11 \lesssim \sin\theta \lesssim 0.14$ (see Section 6.2). Here we fix the inclination angle to $\sin\theta = 0.13$. Figure 4.2 shows the time evolution of the velocity in the y direction, v_y, with $k_n = 2^{-1} \times 10^5$ (red solid line) and $k_n = 2^{17} \times 10^5$ (green dashed line). It is shown that v_y behaves periodically; this period ($\Delta t \sim 4$) corresponds to the period for the particle to get past one particle at the floor. The period hardly depends on the stiffness.

In Fig. 4.3 (a), the k_n dependence of the time averaged kinetic energy, E, is shown. It is shown that the energy is an increasing function of $1/k_n$ in the softer region ($1/k_n \gtrsim 10^{-7}$), but no systematic $1/k_n$ dependence of E exists for $1/k_n \lesssim 10^{-7}$. The average collision rate (number of collisions per unit time) between the slope and the particle , N_w, shows logarithmic dependence on $1/k_n$ in the whole region (Fig. 4.3 (b)). From Fig. 4.3 (c), we also find that the average contact time fraction with the slope, t_w, is a decreasing

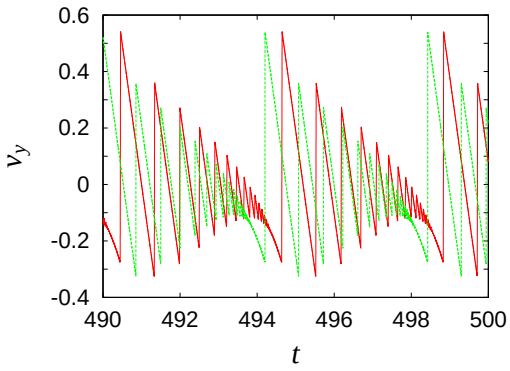

Figure 4.2: Time evolution of v_y with $k_n = 2^{-1} \times 10^5$ (red solid line) and $2^{17} \times 10^5$ (green dashed line).

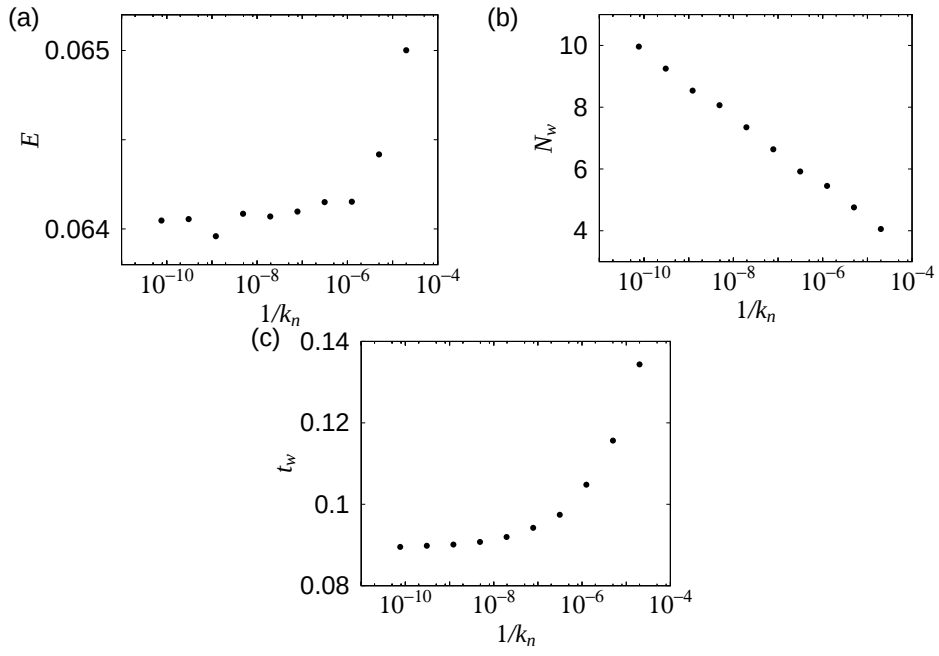

Figure 4.3: The stiffness dependence of (a) the time averaged kinetic energy of the particle E, (b) the collision rate between the slope and the particle N_w, and (c) the contact time fraction between the slope and the particle t_w.

function of k_n in the soft region, but it seems to approach a constant value for large enough k_n.

The logarithmic k_n dependences of N_w and the constant t_w in large k_n region agree with our previous analysis of "inelastic collapse under gravity" in the soft sphere model in Section 4.2. The motion of the particle in one period is as follows; when the particle comes to a bump (a particle attached to the slope), the particle jumps up, bounces on the bump many times, loses the relative velocity, and finally rolls down keeping in contact with the bump. Therefore, the contact time fraction has a finite value even in the hard sphere limit due to the rolling motion at the last part. N_w increases logarithmically in the hard sphere limit as has been expected from Eq. (4.5).

4.3.2 Collisional flow

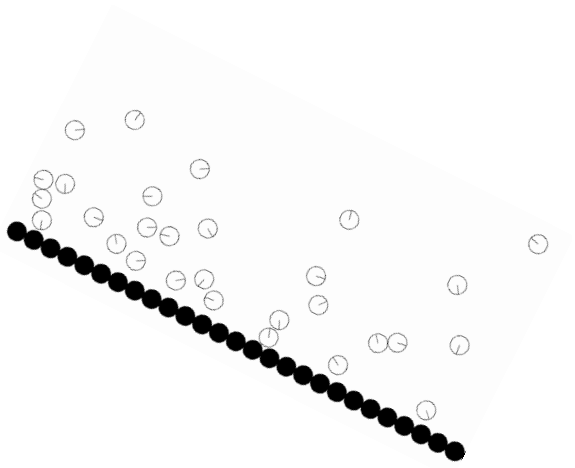

Figure 4.4: A snapshot of the dilute collisional flow.

Next we consider the steady state of the collisional flow. The system considered is shown in Fig. 4.4. The particles are monodisperse, and the slope is made rough as in the single particle case. The periodic boundary condition is adopted in the flow direction (x direction). The length of the slope is $L = 50.1$ and the number of the particles attached to the slope is 50. The number of flowing particles is also 50, namely, the number of the particles per unit length along the slope is about 1. The inclination angle is set to be $\sin\theta = 0.45$. The initial configuration of particles is the row of 50 particles at rest with regular spacing in the x-direction, but each particle

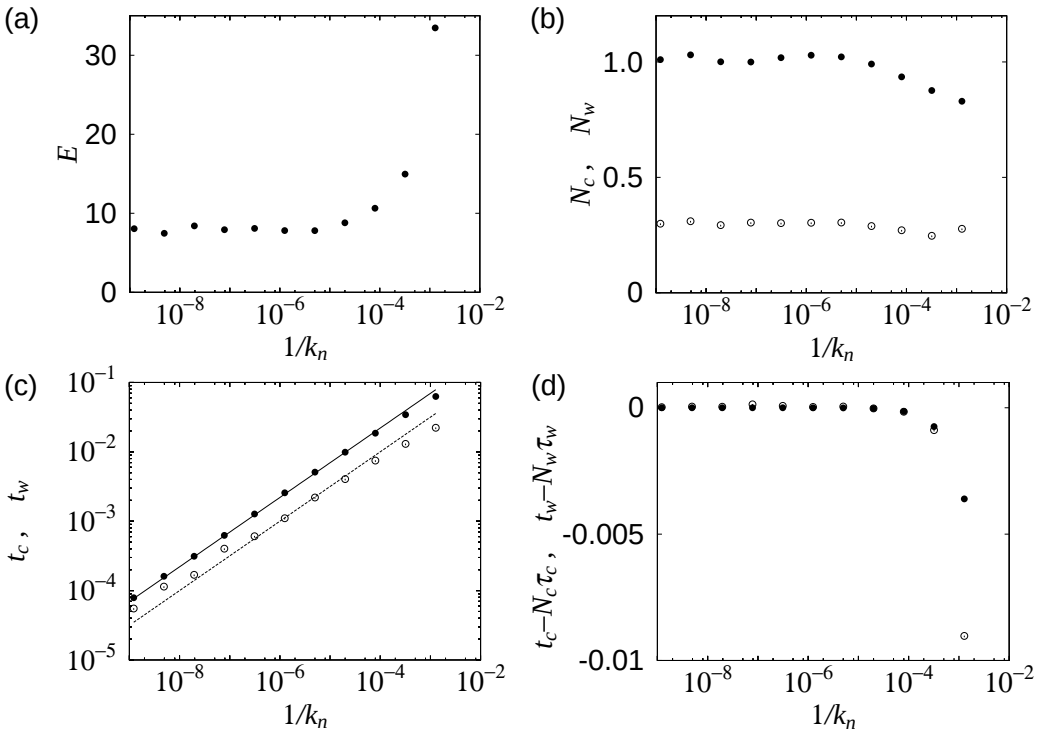

Figure 4.5: The stiffness dependences of (a) the averaged kinetic energy per one particle E, (b) the averaged collision rates between particles N_c (filled circles) and between particles and the floor N_w (open circles), (c) the averaged contact time fractions between particles t_c (filled circles) and between particles and the floor t_w (open circles), (d) the estimated multiple contact time fractions, $t_c - N_c\tau_c$ (filled circles) and $t_w - N_w\tau_w$ (open circles). The solid and the dashed lines in (c) are proportional to $1/\sqrt{k_n}$.

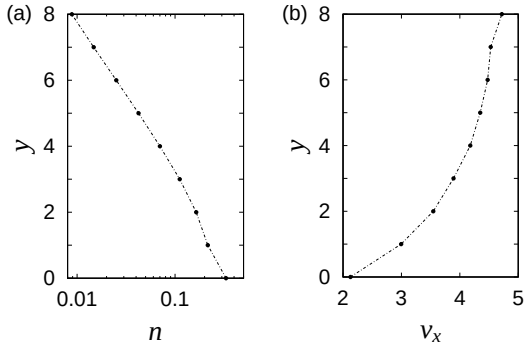

Figure 4.6: The number density profile (a) and the velocity profile (b) of the collisional flow.

is at random height in the y-direction. After a short initial transient, if the total kinetic energy fluctuates around a certain value, we consider it as the steady flow. All the data were taken in this regime and averaged over the time period of 1500.

As can be seen in the snapshot, Fig. 4.4, the particles bounce and the number of particles in contact is very small. In Fig. 4.5 (a), the averaged kinetic energy per one particle, E, is shown. Though E becomes larger as the particles become softer in $1/k_n \gtrsim 10^{-5}$, the systematic dependence of E on k_n disappears for large enough k_n ($1/k_n \lesssim 10^{-6}$). [1] The y-dependence of the average number density and the flow speed in this region are also shown in Fig. 4.6 (a) and (b).

In Fig. 4.5 (b), the average collision rates between particles, N_c (filled circles), and between particles and the slope, N_w (open circles), per particle are plotted v.s. $1/k_n$. Both of them stay roughly constant in the region where E is almost constant, $1/k_n \lesssim 10^{-6}$. The average time fractions during which a particle is in contact with other particles, t_c (filled circles), and in contact with the slope, t_w (open circles), decrease systematically as k_n increases as shown in Fig. 4.5 (c). Both the solid and the dashed lines are proportional to $1/\sqrt{k_n}$, namely, t_c decreases in the same manner as τ_c in Eq. (4.2). Actually, the collision time fractions t_c and t_w converge to $N_c\tau_c$ and $N_w\tau_w$ (τ_w is the duration of a normal collision of a particle and the floor), [2] respectively, in the hard sphere limit. The differences $t_c - N_c\tau_c$ and $t_w - N_w\tau_w$ are plotted in Fig. 4.5 (d) to show that they go to zero very rapidly upon increasing k_n. This means that the interactions of the soft sphere model in the collisional flow regime converge to those of the inelastic hard sphere model with binary collisions.

If we look carefully, however, in the large k_n region in Fig. 4.5 (c), we

[1] The stiffness dependence of the motion of particles discharging from a hopper using discrete element method has been studied by Yuu *et al* [20]. They performed the simulations with three different values of stiffness and found the different behaviors. The comparison with the present results is not simple because of the different set up, but if we normalize their parameter of normal stiffness with the particle mass, the diameter, and the acceleration of gravity, then their values extend over the range where E depends on k_n in our simulations.

[2] When we fix a particle on the slope and employ the same force law as Eq. (3.5), then we have the duration of contact for the normal collision without gravity $\tau_w = \pi/\sqrt{k_n - \eta_n^2/4}$ for identical particles. The force law for the flat boundary that replace $2M$ in Eq. (3.5) by the mass of the colliding particle m gives the same duration of contact with the above one for the normal collision (cf. Appendix B).

can see slight deviation of t_w from the dashed line; it decreases slower than $1/\sqrt{k_n}$. This tendency may indicate that t_w remains finite in the hard sphere limit: Actually, in the event-driven simulation of the hard sphere model, we always found the inelastic collapse as long as the restitution constant between a particle and the floor is less than 1. This suggests that N_w should diverge and t_w should remain finite in the hard sphere limit because of the inelastic collapse due to gravity. The slight deviation of t_w from the dashed line in Fig. 4.5 (c) may be a symptom of it, while we cannot see the logarithmic divergence in N_w.

4.3.3 Frictional flow

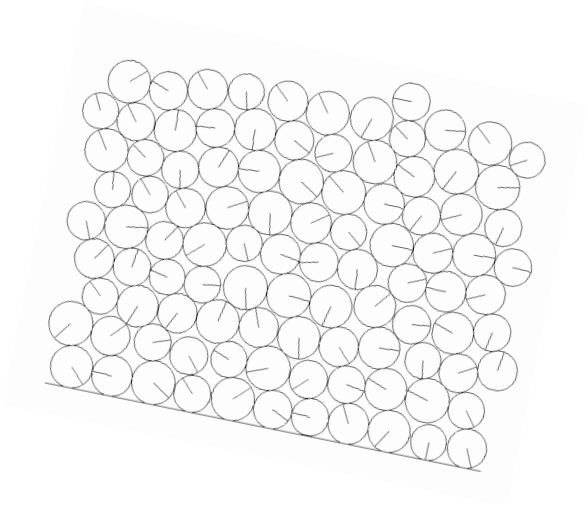

Figure 4.7: A snapshot of the dense frictional flow.

Now we study the steady state of the dense frictional flow. We adopt the flat boundary with slope length $L = 10.02$ and imposed the periodic boundary condition in the flow direction. In order to avoid crystallization, we used the polydisperse particles with the uniform distribution of diameter from 0.8 to 1.0. The number of particles in the system is 100. The inclination angle θ is set to be $\sin\theta = 0.20$ and the initial condition is given in the similar way with the collisional flow. The ten rows of ten particles with regular spacing in the x-direction are at rest with large enough spacings between rows in the y-direction so that particles do not overlap; only the particles in the top row are at random heights in y-direction.

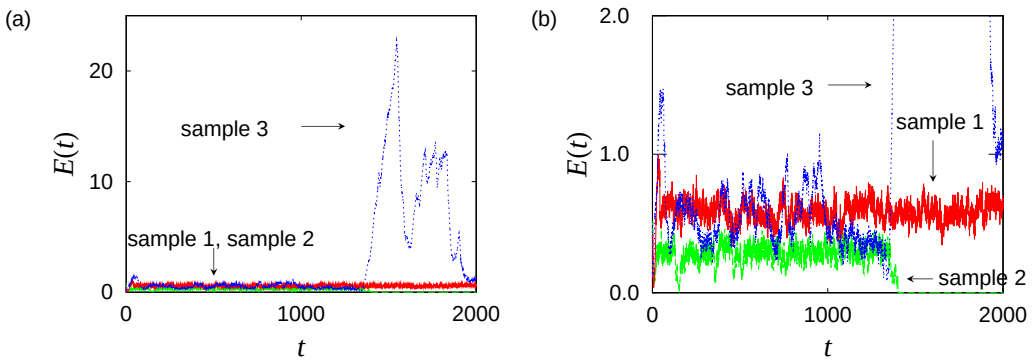

Figure 4.8: Time evolution of the kinetic energy per particle of three samples (sample 1: red solid line, sample 2: green dashed line, sample 3: blue dotted line). (b) is the magnification of (a). Sample 1 with $k_n = 2^{-1} \times 10^5$ shows steady behavior within the threshold. Sample 2 and 3 are with $k_n = 2^{-7} \times 10^5$. Sample 2 shows steady behavior with lower energy for a while but finally stops. $E(t)$ of sample 3 shoots up suddenly at $t \sim 1300$ when one of the particles in the bottom layer runs on other particles.

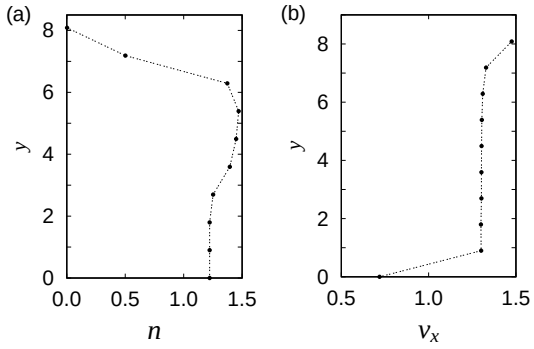

Figure 4.9: The density (a) and velocity (b) profiles of the frictional flow.

It turns out that the steady state is not unique and fluctuation is large. Depending on the initial conditions, the particles may flow with a different value of average kinetic energy, or in some cases, the whole system stops. We presume that this is mainly because the system is not large enough: Grains form a layer structure as in Fig. 4.7, and the flow velocity strongly depends on the configuration of particles in the bottom layer. The time evolutions of the kinetic energy per particle, $E(t)$, of three samples with different configurations in the bottom layer are shown in Fig 4.8. Sample 1 shows stable behavior while sample 2 eventually stops after running with lower energy for some time. Sample 3 shows larger fluctuation with higher energy; the sudden change of $E(t)$ in sample 3 results from the change in the configuration of the bottom layer. This large fluctuation should be averaged out if we could simulate large enough system for long enough time, but the amount of computation is too large especially for the system of stiff particles.

In order to make meaningful comparison out of these largely fluctuating data with a variety of behaviors, we select simulation sequences that come from similar flowing behaviors in the following way. First, we define the steady part of the time sequence in each of the samples as the part where the width of the energy fluctuations is smaller than 0.45 over the time period longer than 500. Second, we exclude the data whose averaged energy is out of the range [0.4,0.8]. [3]

Many of the excluded data by this criterion show quite different flowing behaviors. We use only the data selected from this criterion to calculate time averages of physical quantities.

In the snapshot of the frictional flow, Fig. 4.7, most of the particles seem to be in contact with each other and form a layer structure. The y-dependence of the average density and the flow speed are shown in Figs. 4.9 (a) and (b), respectively. We can see that the relative motion between layers is largest at the bottom and very small in the bulk. The stiffness dependence of the average kinetic energy E is shown in Fig. 4.10 (a); the data are scattered due to the non-uniqueness of the steady state.

Nevertheless, the average collision rates show systematic dependence as shown in Fig. 4.10 (b). Here, the definition of N_c (t_c) is the same as that for the collisional flow, namely, it is the average collision rate (contact time

[3] As for the softest case, $1/k_n = 2^7 \times 10^{-5}$, we had to include the data whose energy goes below the lower limit because of the general tendency that the energy becomes small for the steady part of the very soft region. For $1/k_n \lesssim 10^{-5}$, however, we did not see any general trend in the average energy.

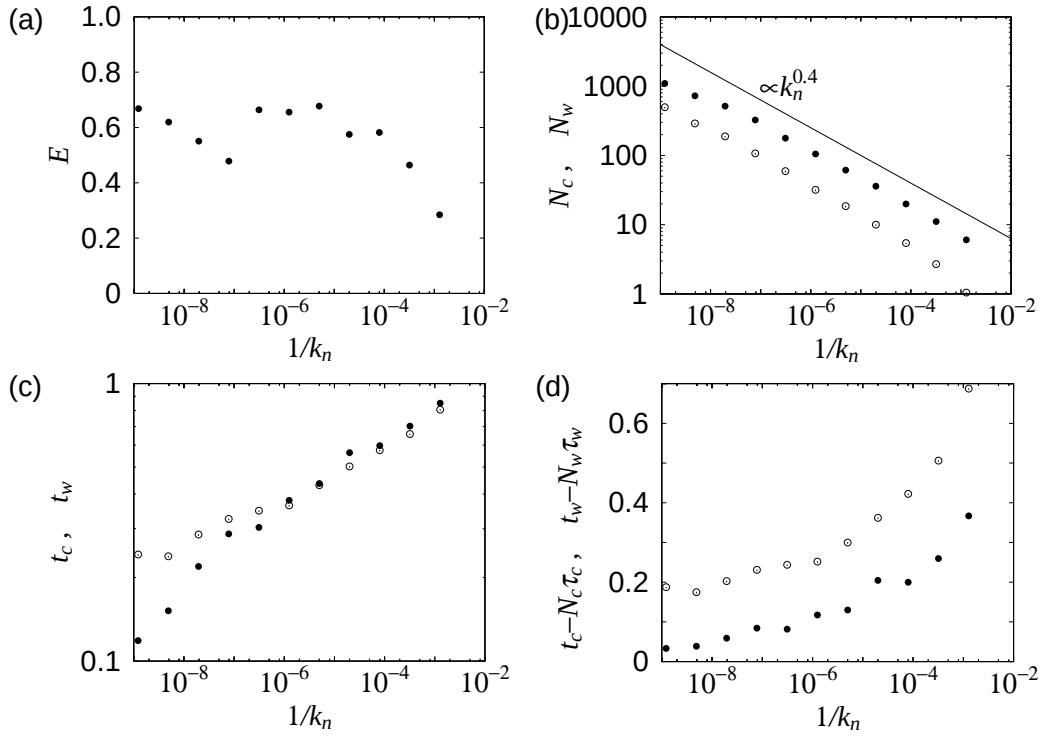

Figure 4.10: The stiffness dependences of (a) the averaged kinetic energy per one particle E, (b) the averaged collision rates between particles N_c (filled circles) and between particles and the floor N_w (open circles), (c) the averaged contact time fractions between particles t_c (filled circles) and between particles and the floor t_w (open circles), and (d) the estimated multiple contact time fractions, $t_c - N_c\tau_c$ (filled circles) and $t_w - N_w\tau_w$ (open circles). In (b) the solid line proportional to $k_n^{0.4}$ is shown for the guide of the eyes.

fraction) between particles *per particle in the system*. N_w (t_w) is defined differently; it is the collision rate (the contact time fraction) between the particles and the slope *per particle in the bottom layer*, because other particles never touch the slope.

In Fig. 4.10 (b), we can see that N_c (filled circles) and N_w (open circles) increase very rapidly as k_n becomes larger: they diverge as a power of k_n. This is quite different from the behavior in the collisional flow in which they are almost constant. Furthermore, this increase is faster than the logarithmic divergence found in the single particle case (see Fig. 4.3 (b)).

The contact time fractions, t_c (filled circles) and t_w (open circles), decrease as shown in Fig. 4.10 (c). The main reason why t_c and t_w decrease is that τ_c and τ_w decrease faster than N_c and N_w, namely, the contact time fractions estimated from the duration of a binary collision, $N_c\tau_c$ and $N_w\tau_w$, continue to decrease. Actually, the decrease of the contact time fraction and the increase of the collision rate are natural because a longer multiple contact breaks up into shorter binary contacts as the particles become stiffer.

These contact time fractions, t_c and t_w, however, do *not* converge to $N_c\tau_c$ and $N_w\tau_w$, respectively. As shown in Fig. 4.10 (d), $t_c - N_c\tau_c$ (filled circles) and $t_w - N_w\tau_w$ (open circles) are very large as compared to those in the collisional flow, even in the stiffest region. The comparison of this with the rapid convergence in the collisional flow regime (Fig. 4.5 (d)) indicates that there remains finite multiple contact time in the hard sphere limit and the interaction in the frictional flow can never be considered as many, or even infinite, instantaneous binary collisions. The particles experience the lasting multiple contact even in the hard sphere limit.

4.4 Summary

The inelastic hard sphere limit of granular flow has been investigated numerically in the steady states of (i) a single particle rolling down the slope, (ii) the dilute collisional flow, and (iii) the dense frictional flow. In (i), it has been found that the "inelastic collapse" between the particle and the slope occurs in the hard sphere limit due to gravity, and the contact time fraction between the particle and the slope remains finite. In (ii), the collision rates, N_c and N_w, are almost constant when particles are stiff enough. The contact time fraction between particles t_c approaches zero as k_n increase in the same manner with the duration of contact for a binary collision τ_c. This

means that the interaction between particles in the hard sphere limit can be expressed by binary collisions in the inelastic hard sphere model. However, the decrease in t_w is slightly slower than $1/\sqrt{k_n}$ in the harder region, which can be a sign of the inelastic collapse between a particle and the slope.

In the case of the frictional flow (iii), the situation is not simple; Although the contact time fractions t_c and t_w decrease upon increasing k_n, the collision rates N_c and N_w increase as a power of k_n, which is faster than the logarithmic divergence found in the single particle case (i). The origin of this power divergence of collision rate does not seem to be simple because it is a property of the steady state, not a particular dynamical trajectory of the system.

The multiple contact time fraction may be estimated by $t_c - N_c\tau_c$ and $t_w - N_w\tau_w$. They were found to be quite large compared to those for the collisional flow, and seems to remain finite even in the infinite stiffness limit; this suggests that the interaction in the frictional flow can never be considered as infinite number of binary collisions. Even in the hard sphere limit, particles experience the lasting multiple contact.

The non-negligible fraction of multiple contact in the hard sphere limit implies the existence of the network of contacting grains even though they are flowing [94]. The models for dense flow should consider the effect of these lasting contacts.

Here we have investigated only the two cases, i.e., the collisional flow and the frictional flow. The system should undergo the transition between the two flows if we change continuously the parameters such as the inclination angle, the roughness of the slope, or the density of particles. It is interesting to investigate how the transition occurs by looking at the quantities measured in this chapter, because their stiffness dependences are qualitatively different in the two flows.

Chapter 5

Collisional Granular Flow as a Micropolar Fluid: Effect of Rotation of Grains

In spite of the long history of research on the granular flows, the theoretical framework for their rheology has not yet been established as stated in Chapter 2. One reason that makes analytical treatment difficult is that the separation between the length scales is not so large; the size of each particle is often comparable with the scale of the macroscopic collective motion. There are many situations in which simple hydrodynamic approaches cannot be used to characterize granular flows [2]. Even when we consider the rapid granular flows [6–10], the coupling between the rotation of each particle and macroscopic velocity field may not be negligible. Then, the behavior of the flow deviates from that of an ordinary Newtonian fluid described by the Navier-Stokes equations.

The micropolar fluid model is a continuum model to describe a fluid that consists of particles with spinning motion [27–30]. The model equations include an asymmetric stress tensor and a couple stress tensor; the model can be a suitable framework to describe granular flows.

In this chapter, we apply a micropolar fluid model to low-density collisional granular flow in which the interaction between particles can be approximated by the binary collisions of the inelastic hard spheres. We adopt a set of constitutive equations that are a simple and natural extension of the Navier-Stokes equations. The inelastic hard sphere picture of the collisional flow, whose validity is confirmed in Chapter 4, allows us to estimate the vis-

cosities by the elementary kinetic theory. We calculate the velocity and the angular velocity profiles for the uniform steady flow on a slope, and demonstrate that the micropolar fluid model reproduces the results of numerical simulations quantitatively.

5.1 Micropolar Fluid Model

It is easy to derive the equations for the number density n, the velocity v_i, and the microrotation field ω_i of a system that consists of identical particles with mass m and moment of inertia I (Appendix A). From the conservation laws of mass, momentum, and angular momentum [29], we obtain

$$\mathrm{D}_t n = -n\partial_j v_j, \tag{5.1}$$

$$mn\mathrm{D}_t v_i = mnf_i + \partial_j S_{ji}, \tag{5.2}$$

$$In\mathrm{D}_t \omega_i = \partial_j C_{ji} + s_i^{(a)}. \tag{5.3}$$

The summation convention applies to repeated subscripts. ∂_i represents a partial derivative with respect to the ith coordinate, $\mathrm{D}_t \equiv \partial/\partial t + v_k\partial_k$ is Lagrange's derivative, and f_i is the body force per unit mass. Here, S_{ij} and C_{ij} are the stress tensor and the couple stress tensor that, respectively, represents the j component of the surface *force* and the surface *torque* acting on the plane perpendicular to the i axis per unit area, and $s_i^{(a)}$ is the torque due to the asymmetric part of the stress tensor defined as

$$s_i^{(a)} = \epsilon_{ijk} S_{jk}, \tag{5.4}$$

where ϵ_{ijk} is the alternating tensor of Levi-Civita.

For the constitutive equation of the stress tensor S_{ij}, we adopt [29]:

$$S_{ij} = (-p + \lambda\partial_k v_k)\delta_{ij} + \mu_s(\partial_i v_j + \partial_j v_i) + \mu_r\left[(\partial_i v_j - \partial_j v_i) - 2\epsilon_{ijk}\omega_k\right], \tag{5.5}$$

with δ_{ij}, Kronecker's delta. The symmetric part of S_{ij} in Eq. (5.5) is the same as the stress tensor in the Navier-Stokes equation with pressure p, shear viscosity μ_s, and bulk viscosity λ. The third term on the right hand side of Eq. (5.5) represents the asymmetric part of the stress tensor due to the difference between the rotation of the mean velocity field and particles' own spin [1]. This gives $\boldsymbol{s}^{(a)} = 2\mu_r[\nabla \times \boldsymbol{v} - 2\boldsymbol{\omega}]$, using Eq. (5.4). The microrotation

[1]The situation where $(\partial_i v_j - \partial_j v_i) = 2\epsilon_{ijk}\omega_k = \text{const.}$ represents the rigid rotation of the whole system, thus the distance between arbitrary two points on constituents does not change. The form of the third term on the RHS of Eq. (5.5) indicates that the rigid rotation produces no internal stress.

viscosity μ_r represents the coupling between the velocity and the microrotation field. For the couple stress tensor C_{ij}, we use the theorem that isotropic second order tensors can be expanded as the trace, the symmetric part, and the asymmetric part of rate of strain tensor for microrotation [29]:

$$C_{ij} = c_0 \partial_k \omega_k \delta_{ij} + \frac{\mu_B + \mu_A}{2}(\partial_i \omega_j + \partial_j \omega_i) + \frac{\mu_B - \mu_A}{2}(\partial_i \omega_j - \partial_j \omega_i), \quad (5.6)$$

where the coefficients of angular viscosity are c_0, μ_A, and μ_B. It should be noted that the dimensions of these coefficients are different from the viscosities in the stress tensor by length-squared because of the difference of the dimensions between S_{ij} and C_{ij} and between v_i and ω_i.

5.2 Estimation of Viscosities

The coefficients of viscosity that appear in Eqs. (5.5) and (5.6) have been derived based on the kinetic theory of three-dimensional spheres with rough surfaces[2] [51, 96, 97]. Here, for later convenience, and also to make the physical meaning of the model clear, we briefly summarize the rough estimate of the viscosities to the lowest order of density for two-dimensional disks using elementary kinetic theory. Let us consider a two-dimensional fluid that consists of identical disks with diameter σ and that is flowing uniformly in the x direction, namely $n = n(y)$, $\boldsymbol{v} = (u(y), 0, 0)$, and $\boldsymbol{\omega} = (0, 0, \omega(y))$. Then we have

$$S_{yx} = \mu_s u'(y) + \mu_r [u'(y) + 2\omega(y)], \quad (5.7)$$

and

$$C_{yz} = \mu_B \omega'(y), \quad (5.8)$$

where the prime denotes a derivative with respect to its argument. Here, S_{yx} (C_{yz}) is the x (z) component of the force (torque) per unit area acting on the plane perpendicular to the y axis.

The coefficient μ_s in Eq. (5.7) corresponds to the kinetic viscosity in dilute gas, which we can find an estimate by kinetic theory in textbooks on statistical physics, e.g. Ref. [98]; S_{yx} represents the net momentum transfer per unit time per unit length by particles crossing the plane $y =$ const., and estimated as $S_{yx} \sim n\bar{v}[mu(y + l) - mu(y - l)] \sim n\bar{v}mlu'(y)$ with the mean

[2] After our work, Hayakawa [95] has derived the transport coefficients in the micropolar equations based on the linearized Boltzmann equation for two-dimensional disks with spinning motion.

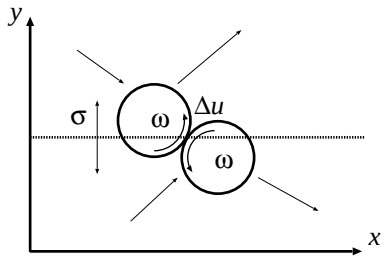

Figure 5.1: A schematic illustration of the situation considered in the estimation of μ_r.

free path l and the root mean square of the velocity in the y direction $\bar{v}$. Thus μ_s is given by

$$\mu_s \sim n\bar{v}ml \sim \frac{1}{\sigma}\sqrt{Tm}, \tag{5.9}$$

where T is the granular temperature (Eq. (2.5)) and the relation $l \sim 1/(n\sigma)$ in two-dimensional system is used.

The coefficient μ_B is estimated by a similar argument to that of μ_s. Because C_{yz} represents the net angular momentum transfer per unit time per unit length due to the microrotation by particles crossing the plane $y =$ const., we can use the argument for μ_s by replacing $u(y)$ and m by $\omega(y)$ and I, respectively. Then μ_B is estimated as

$$\mu_B \sim n\bar{v}Il \sim \sigma\sqrt{Tm}, \tag{5.10}$$

with $I = m\sigma^2/8$ for a two-dimensional disk. As we have mentioned, the dimensions of μ_s and μ_B are different.

For an estimation of μ_r, which gives coupling between particles' own spin and velocity field, we consider the collision of two disks near the plane $y =$ const. [3] A schematic illustration of the situation is shown in Fig. 5.1. If the surface of the disk has some roughness, the momentum tangent to the relative position of the colliding particles at the time of contact is transferred from one particle to another. It is plausible to assume that the tangential momentum transferred in one collision is proportional to m times Δu, the relative tangential velocity of each particle at the contact point. In order to simplify the estimation, let us consider the situation with a uniform velocity

[3] It should be noted that, such a collision process produces the (angular) momentum transfer related to not only μ_r but also μ_s (μ_B). Here, only the lowest order in *each* viscosity is considered, therefore such corrections to μ_s and μ_B are neglected.

field, namely $u'(y) = 0$. [4] Then Δu is given by $\Delta u \sim 2(\sigma/2)\omega(y)$. Because the frequency of collision per unit time per unit length near the plane $y =$ const. with the width σ is proportional to $n^2\bar{v}\sigma^2$ in two-dimension, the momentum transfer across the plane by collisions is estimated as

$$\Delta M \sim n^2\bar{v}\sigma^3 m[2\omega(y)]. \tag{5.11}$$

Comparing Eq. (5.11) and the second term of Eq. (5.7) with $u'(y) = 0$, we obtain

$$\mu_r \sim n^2\bar{v}\sigma^3 m \sim n^2\sigma^3\sqrt{Tm}. \tag{5.12}$$

Summarizing the results above, which are consistent with Refs. [95–97], we get following expressions for the coefficients of viscosity;

$$\frac{\mu_B}{\mu_r} \sim \frac{1}{n^2\sigma^2} \sim l^2, \quad \frac{\mu_s}{\mu_r} \sim \frac{1}{(n\sigma^2)^2} \sim \left(\frac{l}{\sigma}\right)^2. \tag{5.13}$$

It should be noted that, because the dimension of μ_B is different from that of μ_s and μ_r, we need to introduce another length scale to characterize the macroscopic flow behavior in order to compare them. On the other hand, we can see that, when the number density is high enough, μ_r becomes comparable to μ_s, then the coupling between the angular momentum and the linear momentum should play an important role.

5.3 Uniform Steady Solution of Flow on a Slope

Now we present the uniform, steady solution of the micropolar fluid equations (5.1), (5.2), and (5.3) on a slope, and compare the obtained profiles with the result of numerical simulation.

Let us consider the two-dimensional steady flow on a slope under the gravity. We take the x axis in the direction down the slope, and the y axis in the direction perpendicular to the slope. The inclination angle of the slope is θ, and the acceleration of gravity $\boldsymbol{g} = (g\sin\theta, -g\cos\theta, 0)$. In the uniform, steady flow, $mn = \rho = \rho(y)$, $\boldsymbol{v} = (u(y), 0, 0)$, and $\boldsymbol{\omega} = (0, 0, \omega(y))$, therefore

[4] If we consider the situation with $u'(y) \neq 0$, we get $\Delta u = \sigma[u'(y)\cos^2\phi + \omega(y)]$, where ϕ is the angle between the y axis and the vector along the centerline from one particle to another. We need careful calculation in the average process of ϕ, which is beyond elementary kinetic theory.

the equation of continuity (5.1) is automatically satisfied. Eqs. (5.2) and (5.3) reduce to following differential equations:

$$\rho g \sin\theta + \frac{\mathrm{d}}{\mathrm{d}y}\left[\mu_s \frac{\mathrm{d}u}{\mathrm{d}y} + \mu_r\left(\frac{\mathrm{d}u}{\mathrm{d}y} + 2\omega\right)\right] = 0, \tag{5.14}$$

$$-\rho g \cos\theta - \frac{\mathrm{d}p}{\mathrm{d}y} = 0, \tag{5.15}$$

and

$$-2\mu_r\left(\frac{\mathrm{d}u}{\mathrm{d}y} + 2\omega\right) + \frac{\mathrm{d}}{\mathrm{d}y}\left[\mu_B \frac{\mathrm{d}\omega}{\mathrm{d}y}\right] = 0. \tag{5.16}$$

The equation of state for a two-dimensional granular gas has been derived in Ref. [49], but here we adopt the lowest order estimate, namely, $p = \rho T/m$, for simplicity. We also assume the constant temperature $T = \bar{T}$; the validity is of these assumptions is confirmed later in the comparison with the simulation data. With the aid of these assumptions, we obtain the density profile from Eq. (5.15);

$$\rho = \rho_0 \exp\left(-\frac{y}{h}\right), \ h = \frac{\bar{T}}{mg\cos\theta}. \tag{5.17}$$

Then, from the estimate of the coefficients Eq. (5.13), we introduce the non-dimensional constants α_0 and β_0 as

$$\frac{\mu_r}{\mu_s} = \alpha_0 \exp(-2y/h), \quad \frac{\mu_B}{\mu_s} = \beta_0 \sigma^2. \tag{5.18}$$

After integrating Eqs. (5.14) and (5.16) with Eqs. (5.17) and (5.18), we obtain the following relation between the velocity field $u(y)$ and the micro-rotation field $\omega(y)$;

$$\tilde{u}(Y) = -\exp(-Y) - \frac{\beta_0 \epsilon^2}{2}\frac{\mathrm{d}\tilde{\omega}(Y)}{\mathrm{d}Y} + A_0, \tag{5.19}$$

where

$$\tilde{u} = \frac{u}{\rho_0 g h^2 \sin\theta/\mu_s}, \quad \tilde{\omega} = \frac{\omega}{\rho_0 g h \sin\theta/\mu_s}, \tag{5.20}$$

with $Y = y/h$ and $\epsilon = \sigma/h$. Here, A_0 is an integration constant. In the integration of Eq. (5.14), we imposed the boundary condition for stress tensor at the free surface, $\lim_{y\to\infty} S_{yx} \to 0$. From Eqs. (5.16) and (5.19), we have

$$\frac{\mathrm{d}^2\tilde{\omega}(Y)}{\mathrm{d}Y^2} - 2\frac{\alpha_0 \exp(-2Y)}{\beta_0 \epsilon^2}\left[\frac{\exp(-Y) + 2\tilde{\omega}(Y)}{1 + \alpha_0 \exp(-2Y)}\right] = 0. \tag{5.21}$$

Its general solution is given as the sum of a particular solution $\tilde{\omega}_p$ and two homogeneous solutions $\tilde{\omega}_1$ and $\tilde{\omega}_2$ by

$$\tilde{\omega}(Y) = A\tilde{\omega}_1(Y) + B\tilde{\omega}_2(Y) + \tilde{\omega}_p(Y), \tag{5.22}$$

with integration constants A and B. Changing the variable from Y to $\nu = \exp(-Y)$, we can obtain the expressions

$$\tilde{\omega}_p = \sum_{k=1}^{\infty} a_{2k+1}\nu^{2k+1} \quad \text{with} \quad a_3 = \frac{2\alpha_0}{9\beta_0\epsilon^2}, \quad a_{2k+1} = f_{2k+1}a_{2k-1}, \tag{5.23}$$

$$\tilde{\omega}_1 = \sum_{k=0}^{\infty} b_{2k}\nu^{2k} \quad \text{with} \quad b_0 = 1, \quad b_{2k} = f_{2k}b_{2k-2}, \tag{5.24}$$

and

$$\begin{aligned} \tilde{\omega}_2 &= \tilde{\omega}_1 \log\nu + \sum_{k=1}^{\infty} c_{2k}\nu^{2k} \\ &\text{with} \quad c_0 = 0, \quad c_{2k} = f_{2k}c_{2k-2} - \frac{\alpha_0}{k^3}\left[\frac{1}{\beta_0\epsilon^2} + k - 1\right] b_{2k-2}, \end{aligned} \tag{5.25}$$

where

$$f_k \equiv \frac{\alpha_0}{k^2}\left[\frac{4}{\beta_0\epsilon^2} - (k-2)^2\right]. \tag{5.26}$$

Note that $\tilde{\omega}_p$ and $\tilde{\omega}_1$ are regular but $\tilde{\omega}_2$ diverges at $\nu = 0$ ($Y \to \infty$).

Now we show that the solution obtained from the micropolar fluid model can quantitatively reproduce the results of numerical simulation. We use the two dimensional DEM simulation data of collisional granular flow of identical particles on a bumpy slope, which is presented in Chapter 6; the detail of the simulation setup is given in that chapter. In the following, all quantities are given in dimensionless form with the particle mass m, the particle diameter σ, and the time unit $\tau = \sqrt{\sigma/g}$.

We used the data of the simulation with inclination $\sin\theta = 0.45$, system size $L = 1002$, and number of flowing particle $N = 1000$. In the simulation, uniform collisional flow is realized during $500 \lesssim t \lesssim 2000$ where t is the time as can be seen in Fig. 6.4. In order to determine the profiles of the mean quantities describing the flow, we divide the space into layers which are one particle diameter wide parallel to the slope, calculate the averages inside layers, and then average the data over the time within the uniform flow, $1000 \leq t < 1500$. The slope is made bumpy by attaching identical

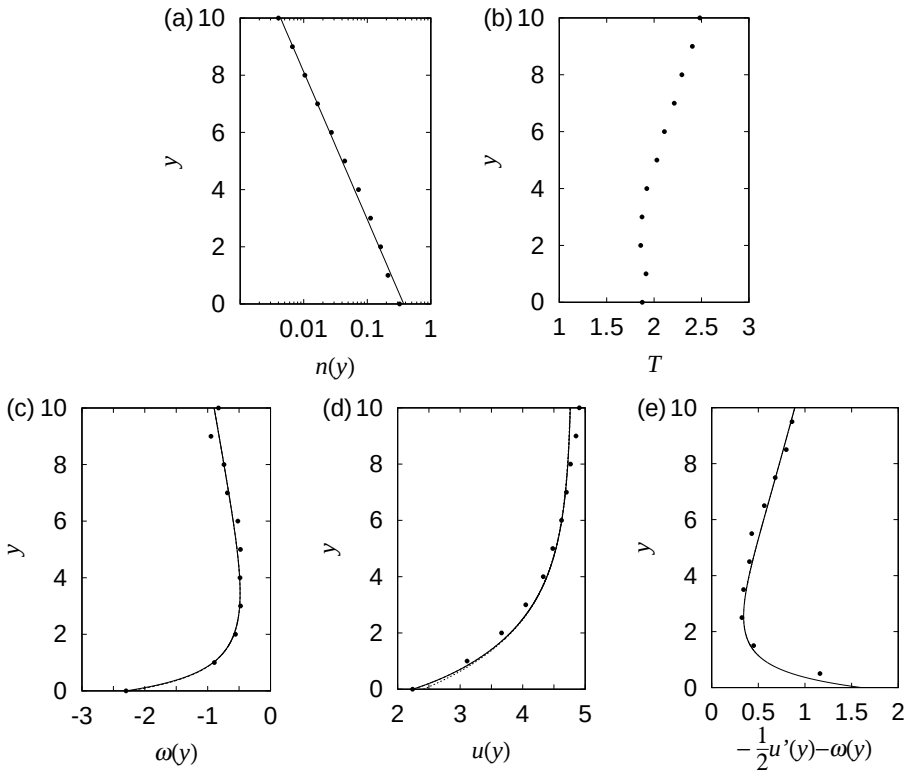

Figure 5.2: Properties of the uniform flow. The filled circles are obtained from the simulation data, and the solid line is the uniform steady solution of the micropolar fluid equations. (a) The number density profile $n(y)$. (b) The temperature profile $T(y)$. (c) The angular velocity profile $\omega(y)$. (d) The velocity profile $u(y)$. The dotted line represents the solution of Navier-Stokes equations without angular velocity. (e) The difference between the rotation of the bulk velocity field and the microrotaion, $(\frac{1}{2}\nabla\times\boldsymbol{v}-\boldsymbol{\omega})_z = -\frac{1}{2}u'(y)-\omega(y)$.

disks, and the origin $y = 0$ is taken one diameter above from the top of the disks attached to the slope.

Now let us compare our result from the micropolar fluid model with the simulation data. First, we confirmed that the number density profile can be well-fitted by Eq. (5.17) with $h = 2.24$ as shown in Fig. 5.2 (a), namely, $\bar{T} \sim 2.0$. This value is close to the averaged value of T shown in Fig. 5.2 (b), and the variation of T in the y direction is small compared to the exponential variation of n; these facts allow us to use the equation of state of ideal gas and the assumption of the constant temperature as the first approximation.

In order to fit the solutions (5.19) and (5.22) to the simulation data, we determine the boundary values $u(0)$ and $\omega(0)$ from the data and treat α_0, β_0, μ_s/ρ_0 and $\omega'(0)$ as fitting parameters. From Fig. 5.2 (c), we can see that the micropolar fluid equations reproduce the angular velocity quantitatively. Here, the value of parameters are $\alpha_0 \sim 0.10$, $\beta_0 \sim 0.12$, $\mu_s/\rho_0 \sim 0.95$, and $\omega'(0) \sim 2.9$. The velocity profile $u(y)$ can also be well-reproduced by the solution (5.19) as shown by the solid line in Fig. 5.2 (d); however, because the density is low, the deviation of the velocity profile from the solution of the Navier-Stokes equation without angular velocity, i.e. $\tilde{u}(Y) = -\exp(-Y) + A_0$, is small, which is also shown in Fig. 5.2 (d) by dotted line. Actually, we have checked that the data can be reasonably fit with any small value of α_0, as long as α_0/β_0 is chosen appropriately. However, it is significant that the solution (5.22) can reproduce the sharp variation of $\omega(y)$ over only a few diameters near the base.

The more important thing is that the mean spin $\boldsymbol{\omega}$ deviates systematically from the rate of bulk rotation $\frac{1}{2}\nabla\times\boldsymbol{v}$, and that the micropolar fluid model can reproduce this deviation. In Fig. 5.2 (e), we see that the deviation is large near the base, because each particle is forced to rotate by the collision with the slope. This result indicates the importance of the couple stress near the boundary, as pointed out by Champbell [48]. This deviation may produce the velocity profile different from the Newtonian fluids described by the Navier-Stokes equation due to the coupling between the spin of each particle and the linear velocity field. On the other hand, it seems the deviation also becomes large in the region far from the boundary. The reason is that the microrotation field in this region is dominated by a small number of particles spins that are generated by collisions with the boundary.

5.4 Summary

In summary, the micropolar fluid model has been applied to a collisional granular flow with relatively low density. It has been demonstrated that the solution for uniform, steady flow on an inclined surface reproduces the results of numerical simulation.

Because the density is low, the ideal gas assumption for the equation of state and the estimation of the viscosity from the elementary kinetic theory work well. In order to apply the model to denser collisional flows, we need a systematic extension of the theory using, for example, Enskog theory. This has already been done in the context of polyatomic fluids for completely rough spheres without energy dissipation [96, 99] and it should be possible to extend such results to the dissipative case [51]. The equation of state for dense granular gas has also been discussed recently [8, 51].

On the other hand, the coupling between the particle spin and the velocity field becomes stronger in dense frictional flows [100–102]. In some research, the mechanics of granular media in dense quasi-static situation is considered based on the micropolar or Cosserat theory [103, 104]. The concepts in micropolar mechanics may be helpful to understand the mechanics of granular media, not only in the collisional flow regime but also in the denser situation.

Chapter 6

Steady State and its Instability of Low-Density Collisional Flow

Most of researches on the collisional granular flow on a slope focus upon the property of the steady uniform flow as referred in Chapter 2; in those researches, the depth dependence of the flow properties such as velocity or density profile is investigated, assuming that the flow is uniform in the direction along the slope. It is known, however, that the granular materials have the tendency to cluster due to the inelastic collision, which causes the formation of density waves in the case of granular flow in a vertical pipe [31, 32]. Therefore, it is natural to expect that this tendency will cause some instability in the uniform flow on a slope.

Granular flow of an independent particle, or a single particle behavior, has been studied as summarized in Section 2.1. It has been found to show three types of motion depending on the inclination angle and roughness of the slope; they are the static state (regime A), the steady motion with a constant average velocity (regime B), and the accelerated motion (regime C). When we increase the number of flowing particles, however, all the particles stop with the inclination angle in regime B because the kinetic energy of the steady motion is not large enough to overcome the energy loss through inelastic collisions with other particles. It will give us an insight on the many-body effect in the low-density granular flow to investigate how the single particle picture is modified upon increasing the density of flowing particles.

In this chapter, we study how the single particle picture is modified in the collisional flow with finite density by particle collisions. Based on numerical simulations, we determine the parameter region where the uniform collisional flow is realized with the finite density. Then we examine the stability of the

uniform flow.

6.1 Simulation Setup

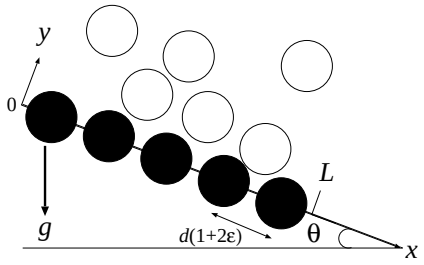

Figure 6.1: A schematic illustration of the system geometry.

k_n	k_t	η_n	η_t	μ
5×10^4	$(5 \times 10^4)/3$	35.68	35.68/3	0.5

Table 6.1: Parameters used in the simulations.

We employed the two dimensional DEM introduced in Section 3.1. The particles are monodisperse with the diameter σ and the mass m. Each particle is also subject to the gravity, and the gravitational acceleration is given by $\boldsymbol{g} = g(\sin\theta, -\cos\theta)$. The surface of the slope is made rough by attaching the particles identical to the moving ones with spacing 0.002σ (Fig. 6.1). The periodic boundary condition is imposed in the x direction. The system size L is determined by the number of the particles attached to the slope n_s as $L = 1.002\sigma n_s$.

All quantities which appear in the following are given in the nondimensionalized form in terms of the length unit σ, the mass unit m, and the time unit $\tau = \sqrt{\sigma/g}$. The parameters used in the simulations are tabulated in Table 6.1. These parameters give the restitution coefficients $e_n = \beta = 0.7$ from the relations (3.19) and (3.23), and the duration of contact $\tau_c \sim 1 \times 10^{-2}$ from (3.18). We integrated the equations of motions using the predictor-corrector method in the third order with a constant time step $dt = 1 \times 10^{-4}$.

6.2 Steady Flow from the Single Particle Limit

We first investigate how the uniform collisional flow appears when we increase the density of flowing particles from the one particle limit.

As we have referred in Section 2.1, a single particle behavior depends on the value of θ for a fixed roughness of the slope. It is known, however, that the boundary between the regime B (the constant velocity regime) and C (the acceleration regime) is not sharp; there is a parameter region where the particle can attain steady state or can accelerate, depending on the initial condition. We should also note that, when the initial kinetic energy of the particle is too small, the particle may stop in the regime B and in part of the regime C. In the present model with the parameters in Table 6.1, it turns out that the regime A roughly corresponds to the region $\sin\theta \lesssim 0.11$, the regime B to $0.11 \lesssim \sin\theta \lesssim 0.14$, and the regime C to $0.16 \lesssim \sin\theta$.

Now we focus on what happens when the number of moving particles N is increased with the finite L. It is easy to expect that the dissipation becomes larger upon increasing N, because the collisions between particles or a particle and the slope become more frequent. Therefore it is obvious that all the particles will stop irrespective of the initial condition if θ is in the regime A. Even for any θ within the regime B, it turns out that the collisions between particles eventually stop all the particles.

We examine closely the flowing behavior for the larger inclination angle θ in the regime C. The situation is presented by showing the simulations with $\sin\theta = 0.45$ and $L = 20.04$. We set the initial condition as follows:

$$x_i(0) = (L/N)(i-1),\ y_i(0) = (1+2\epsilon) + \alpha\xi_i, \tag{6.1}$$

$$u_i(0) = 0,\ v_i(0) = 0,\ \omega_i(0) = 0, \tag{6.2}$$

where $x_i(t)$ ($y_i(t)$) and $u_i(t)$ ($v_i(t)$) are the coordinate and the velocity of center of mass of the ith particle at time t in the x (y) direction, respectively. $\omega_i(t)$ is the angular velocity of particle i at time t. ξ_i is a random number uniformly distributed over the interval [0, 1]. The appropriate value of α is a few times the diameter, and we adopted $\alpha = 3 \sim 4$ in actual simulations. In the following, we define the 'density' of the particles as $\bar{\rho} = N/L$. In the simulations with $L = 20.04$, we do not observe non-uniformity along the slope in the particle distribution, therefore the parameter $\bar{\rho}$ is enough to describe the situation. In order to characterize the qualitative difference of accelerated behavior in the regime C and the uniform flow, we investigate

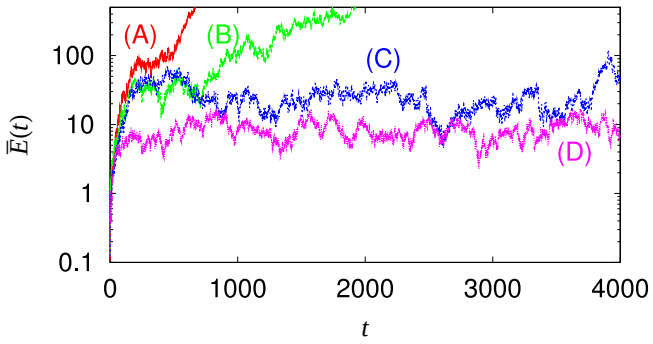

Figure 6.2: The semi-log plot of $\bar{E}(t)$ for (A)$\bar{\rho} = 0.50$, (B)$\bar{\rho} = 0.60$, (C)$\bar{\rho} = 0.65$, and (D)$\bar{\rho} = 1.00$, with $\sin\theta = 0.45$ and $L = 20.04$. $\bar{E}(t)$ continues to grow when $\bar{\rho} \leq 0.60$, while it is bounded when $\bar{\rho} \geq 0.65$.

the $\bar{\rho}$ dependence of the averaged kinetic energy $\bar{E}(t)$ defined as

$$\bar{E}(t) = \frac{1}{N}\sum_{i=1}^{N} E_i(t), \tag{6.3}$$

where $E_i(t)$ is the kinetic energy of the ith particle at time t;

$$E_i(t) = \frac{1}{2}m\left[u_i(t)^2 + v_i(t)^2\right] + \frac{1}{2}I\omega_i(t)^2, \tag{6.4}$$

with $I = m\sigma^2/8$.

In Fig. 6.2, the time evolutions of $\bar{E}(t)$ are shown for several values of $\bar{\rho}$. When $\bar{\rho}$ is small ($\bar{\rho} \leq 0.60$), $\bar{E}(t)$ grows rapidly and continuously, but the growth rate become smaller as $\bar{\rho}$ increases. In this region, each particle jumps and rarely collides with each other. When $\bar{\rho} \geq 0.65$, $\bar{E}(t)$ still grows rapidly in early stage, but its long-time behavior seems to be bounded and fluctuate around a constant value. In this case each particle also jumps, but often collides with other particles and is prevented from jumping up infinitely. Based on this observation, we define the uniform flow in the low-density limit as the flow which is uniform along the flow direction with the value of $\bar{E}(t)$ being bounded, namely the energy dissipation due to inelastic collisions balances with the energy gain from the gravity.

The average value of the kinetic energy $\bar{E}$ in the uniform flow should be related to X, the distance between collisions along the slope, by $(1-e^2)\bar{E} \sim mgX\sin\theta$, because the energy gain by the gravitation should balance with the loss due to inelastic collisions. The simulation shows the typical value

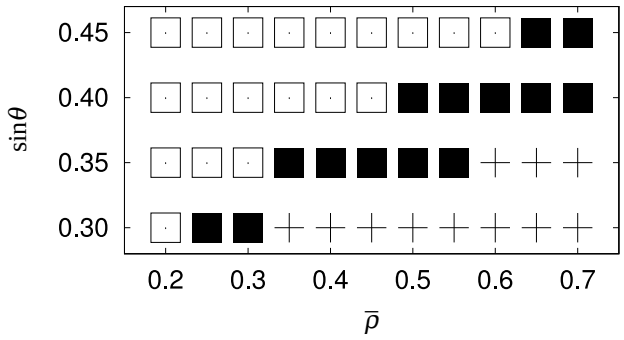

Figure 6.3: The 'phase diagram' obtained from the simulations with $L = 20.04$. The accelerated regime (open box), the uniform flow regime (filled box), and the regime where all the particles stop (plus) are shown when more than 50 % of trials result in the corresponding behavior.

of X to be $O(1) \sim O(10)$ in the uniform flow, thus we expect $\bar{E}$ to be $O(1) \sim O(10)$. On the other hand, $\bar{E}$ diverges in the accelerated regime.

Figure 6.3 shows the 'phase diagram' summarizing the behavior in terms of θ and $\bar{\rho}$ obtained from numerical simulations. In order to obtain the diagram, 10 simulations with $L = 20.04$ were done for each θ and $\bar{\rho}$. We identify the three behaviors, namely (i) accelerated motion, (ii) uniform flow, and (iii) static state where all the particles come to rest, by the following criterion; the system is determined to be in the accelerated motion (in the static state) if $\bar{E}(t)$ exceeds 500 (becomes zero) by $t = 20,000$. It is determined to be the uniform flow if neither of them happen. The final behavior sometimes depends on the initial condition. This, we believe, is due to the finite size effect. Each point in Fig. 6.3 is determined to be in one of these regimes if more than 50 % of the trials show the one of the above behaviors. It is expected that, if we could take the $L \to \infty$ limit with fixed $\bar{\rho}$ with keeping the particle distribution uniform along the slope, such initial condition dependence should disappear.

6.3 Spontaneous Density Wave Formation

Now we examine the stability of the uniform flow by taking the system size large enough to observe non-uniformity along the slope. First we show the simulation results of the flow in the system with $\sin\theta = 0.45$, $L = 1002$ and

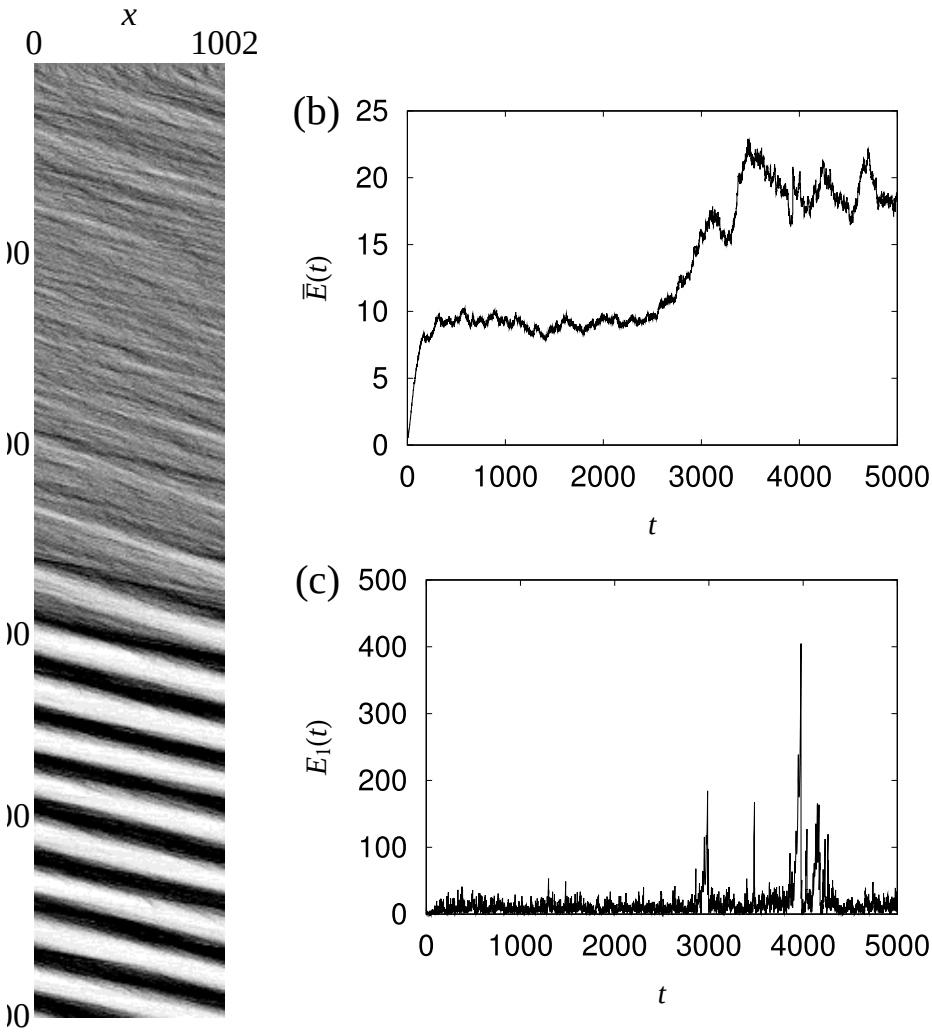

Figure 6.4: (a) Spatiotemporal diagram of the local density. Darker region indicates the higher density region. (b) The time evolution of the averaged kinetic energy $\bar{E}(t)$. (c) The time evolution of the kinetic energy of one particular particle $E_1(t)$.

$N = 1000$, i.e. $\bar{\rho} = 1.0$. The initial condition is also given by Eq. (6.2), therefore the particles are uniformly distributed along the slope at first.

Figure 6.4 (a) shows the spatiotemporal diagram of the local density along the slope; the vertical axis is the time t, the horizontal axis is the coordinate along the slope x, and the darker region represents the higher density region. The y coordinates of the particles are not taken into account in that diagram.

In early stage, the density is almost uniform along the slope ($300 \lesssim t \lesssim 2000$), namely uniform flow is realized. Then relatively large fluctuation of density grows in the course of time ($2000 \lesssim t \lesssim 3000$); this means the clustering behavior is triggered by the fluctuation. Finally system separate into the high density region and the low density region, namely one large cluster is formed ($t \gtrsim 3000$). This cluster travels the system with almost constant velocity because of the periodic boundary condition; we can see that the cluster is stable once it is formed.

The time evolutions of the kinetic energy averaged over all particles, $\bar{E}(t)$, and that of one particular particle, $E_1(t)$, are also shown in Figs. 6.4 (b) and (c), respectively. Both of them are almost constant in the stage of uniform flow. Then $\bar{E}(t)$ increases in $2000 \lesssim t \lesssim 3000$. In $t \gtrsim 3000$, the fluctuation of $E_1(t)$ becomes considerably large, and $\bar{E}(t)$ begins to fluctuate around another constant value which is larger than the one in the stage of uniform flow. The reason why the kinetic energy increases when a cluster is formed can be understood as follows: When the cluster is formed, the region with the density lower than the threshold value to maintain the steady flow (~ 0.65 in the case of $\sin\theta = 0.45$, see Fig. 6.3.) appears locally, and particles in such a spatial region can be highly accelerated. However, the particle will be caught in the cluster sooner or later, and then quickly lose its kinetic energy. This mechanism maintains the moving cluster, and results in the large fluctuations in $E_1(t)$.

The situations are clearer in Figs. 6.5, which show the snapshots of the particle configuration and the local density (number of particles per unit length) at (a) $t = 0$ (initial condition), (b) $t = 1500$ (uniform flow stage), and (c) $t = 5000$ (clustering stage). The red circles in the figures express the particles, but the diameters are ten times larger than the real scale for better sight. The initial condition is completely uniform along the slope as shown in Fig. 6.5 (a). In the uniform flow stage, Fig. 6.5 (b), the uniform particle distribution is realized with some fluctuation. Figure 6.5 (c) of the clustering stage shows that the particles in the low density region are jumping up, while those in the dense region stay close to the floor.

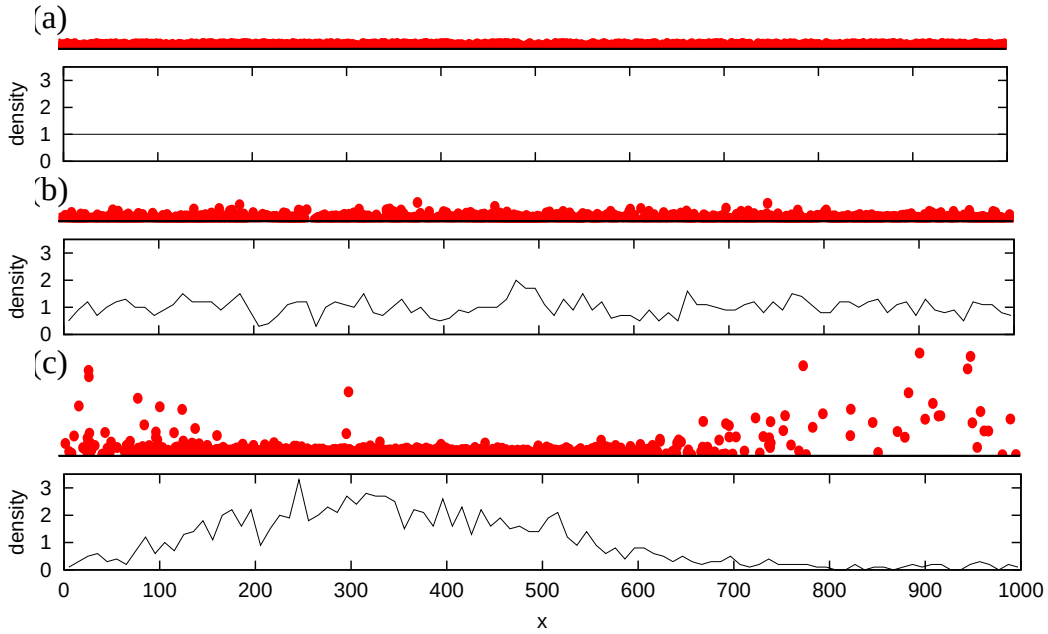

Figure 6.5: The snapshots of the particle configuration (upper figures) and the local density (lower figures) at $t = 0$ (a), $t = 1500$ (b), $t = 5000$ (c). The red circles in the upper figures express the flowing particles, but the diameters of circles are ten times larger than the real scale for better sight.

We also find that the instability depends on the system size L and the "density" $\bar{\rho}$. In Figs. 6.6, spatiotemporal diagrams of the local density with the different values of L and $\bar{\rho}$ are shown. From the comparison of Fig. 6.4 (a), Figs. 6.6 (a) and (b), which are the simulation results with $\bar{\rho} = 1.0$ but different L, we can see that the instability becomes weaker for smaller system sizes. From Fig. 6.6 (a), (c), and (d), which are the results with $L = 501$ but different $\bar{\rho}$, we find that the higher the density is, the more stable the uniform flow is. It can also be seen that, even though the clear cluster formation has not been found in Fig. 6.6 (a), the density fluctuation is quite large. We have also simulated the system with the same L and N as in Fig. 6.6 (a) but *with the initial configuration with large inhomogeneity along the flow direction* (Fig. 6.6 (e)). It is found that, a cluster is formed after a while, but it almost disappears when the head and the tail of the cluster collide through the periodic boundary condition ($3000 \leq t \leq 4000$).

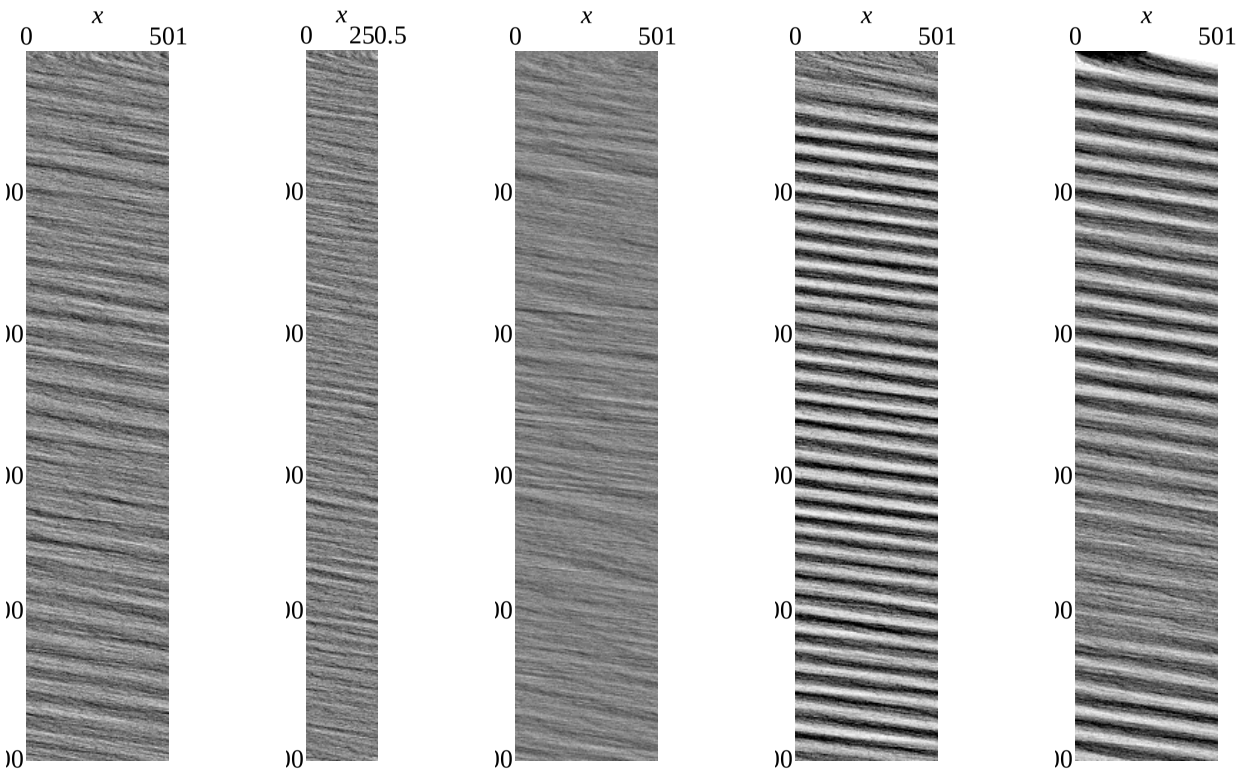

Figure 6.6: Spatiotemporal diagrams of local density with the different values of L and $\bar{\rho}$. The darkness is adjusted so that uniform distribution is shown by grey region in each figure. (a) $N = 500$, $L = 501$, $\bar{\rho} = 1.0$. (b) $N = 250$, $L = 250.5$, $\bar{\rho} = 1.0$. (c) $N = 1000$, $L = 501$, $\bar{\rho} = 2.0$. (d) $N = 375$, $L = 501$, $\bar{\rho} = 0.75$. (e) $N = 500$, $L = 501$, $\bar{\rho} = 1.0$, with the initial configuration with large inhomogeneity along the flow direction.

6.4 Summary

We have examined the two-dimensional granular flow on a rough slope in the collisional flow regime by numerical simulations. It was shown that the mutual collisions among particles stabilizes the flow even in the accelerated regime for a single particle system. The phase diagram was determined for the accelerated, uniform flow, and stopping regime in terms of the particle density $\bar{\rho}$ and the inclination angle θ for a particular system size. The stability of uniform flow was also examined and we found that a large single cluster appears spontaneously out of a uniform initial state. It was shown that the smaller the particle density is, or the larger the system size is, the less stable the uniform flow is.

In the case where the uniform flow was unstable (Figs. 6.4(a) and 6.6(d)), the fluctuation grew up to form a large cluster. The final state was that one stable cluster travels the system with almost constant velocity; it was due to the finite size effect under the periodic boundary condition. The reason why the formed cluster was almost broken in the case of $L = 501$ and $\bar{\rho} = 1.0$ (Fig. 6.6(e)) was that the head and the tail of the cluster interacted through the periodic boundary condition, namely, it was also the finite size effect.

Based on these observations, we guess that, if we perform a simulation or an experiment of initially uniform flow in a very long system under an open boundary condition, the small clusters merge to form larger clusters as they go downstream. It is a future issue to investigate the instability in more realistic situations [1].

The spontaneous cluster formation out of uniform flow is seen also in the granular flow through a vertical pipe [31, 32] and in the traffic flow on a freeway [105–107]. It is an interesting problem to find out whether those phenomena and the cluster formation found here have a common mathematical structure at phenomenological level.

[1] In the wave formation observed in a recent experiment of shallow granular flow on a slope [61], it has been found that the wavelength becomes longer in the downstream.

Chapter 7

Concluding Remarks

In this thesis, we investigated the fundamental properties of the gravitational granular flow. We chose the flow on a slope as a model system because, in spite of its simple setup, all types of granular flows are realized by changing the inclination angle, the roughness of the slope, or the density of particles. It is a system suitable for the comprehensive research on granular flow.

We examined the particle stiffness dependence of the steady flows numerically by taking the inelastic hard sphere limit of the soft sphere model. In the case of the collisional flow, the collision rate is almost constant and the contact time fraction approaches to zero, which means the interaction between particles converges to the binary collisions in the inelastic hard sphere model. On the other hand, the collision rate diverges in the power law of the stiffness parameter in the frictional flow. The estimated time fraction for the multiple or the sustained contact remains finite even in the hardest case. This suggests that the interaction in the frictional flow can never be expressed by the binary collisions: even in the hard sphere limit, particles experience the lasting multiple contact.

The inelastic hard sphere picture of the granular material in the collisional flow regime allows us to use the kinetic theory and the hydrodynamic model. We applied the micropolar fluid model to the collisional granular flow in which the effect of the spinning motion of particles is incorporated. The adopted constitutive equations were the straightforward extension of the Navier-Stokes equation. We used the simple estimate of the viscosities based on the elementary kinetic theory, and obtained the analytical solution of the steady flow on a slope. It was demonstrated that the solution reproduces quantitatively the deviation of the particle spin from the vorticity of the mean velocity field in the numerical simulation.

It was shown by the numerical simulation that the uniform collisional flow exhibits the dynamical instability. We determined the parameter region where the collisional uniform flow is realized with the finite density for a particular system size. Then we performed the simulation in the very long system, and it was found that the uniform flow shows the clustering instability. It was demonstrated that the uniform flow is less stable for the longer system size and/or the lower density.

These results are informative for linking the understandings of the low-density rapid flow to the dense slow flow. The qualitative difference of the stiffness dependence between the collisional flow and the frictional flow is helpful to quantify the dominant interaction in the situation where both the inelastic collision and the sustained contact occurs. The coupling between the spinning motion of particles and the mean velocity becomes stronger for the denser flow. The clustering instability results in coexistence of dense regions and dilute regions. We hope that the future extension of our research will help to understand the nature of transition between the collisional flow and the frictional flow, and finally to construct the comprehensive theory of granular flow.

Acknowledgement

I would like to express my sincere gratitude to my adviser, Prof. Hiizu Nakanishi, for his patient and continuous encouragement, valuable stimulating discussions, and critical comments on the present thesis and all of my studies. His dedicated guidance has been instrumental in my academic development. I am also grateful to Prof. Hisao Hayakawa for his encouragement, helpful suggestions, and collaborations. I learned a lot about granular physics through fruitful discussions with him. The encouragement, valuable discussions and comments on the present thesis by Prof. Hiroshi Kawai and Prof. Masayuki Tokita are also acknowledged very much.

Thanks are also due to Prof. Kiyohide Nomura and Dr. Yumino Hayase for their helpful comments on my studies and computation. I am very thankful to Prof. Takashi Odagaki, Prof. Akira Yoshimori, and Dr. Jun Matsui for valuable comments on the thesis work and advice on my studies. I would like to thank Mr. Masashi Torikai, Dr. Masaharu Isobe, and all members of statistical physics and condensed matter theory research groups at Kyushu University for valuable discussions and friendships.

I would like to acknowledge the warm hospitality of people in Kyoto during my stay at Yukawa Institute for Theoretical Physics in winter, 2001, where part of my thesis work has been carried out.

Part of the computation in this work has been done using the facilities of the Supercomputer Center, Institute for Solid State Physics, University of Tokyo. This research is partially supported by Hosokawa powder technology foundation and Grant-in-Aid for JSPS Research Fellows.

Finally I gratefully thank my family and friends for their warm supports and encouragement.

Appendix A

Derivation of the Micropolar Fluid Equations

We outline the derivation of the micropolar fluid equations (5.1) - (5.3) from the conservation laws of mass, momentum, and angular momentum. The derivation here is based on Ref. [29].

A.1 Equation of Continuity

We consider a volume $V(t)$ which moves with the fluid and whose surface is $\Omega(t)$.

From the conservation law of mass, we obtain

$$\frac{\mathrm{d}}{\mathrm{d}t}\int_{V(t)} \rho \mathrm{d}\boldsymbol{r} = 0. \tag{A.1}$$

Using the relation

$$\frac{\mathrm{d}}{\mathrm{d}t}\int_{V(t)} G(\boldsymbol{r},t)\mathrm{d}\boldsymbol{r} = \int_{V(t)} [\partial_t G + \boldsymbol{v}\cdot\nabla G + G\nabla\cdot\boldsymbol{v}]\mathrm{d}\boldsymbol{r} \tag{A.2}$$

for an arbitrary scalar function $G(\boldsymbol{r},t)$ [108], we get the equation of continuity;

$$\partial_t\rho + \nabla\cdot\rho\boldsymbol{v} = 0 \Leftrightarrow \frac{\mathrm{D}\rho}{\mathrm{D}t} + \rho\nabla\cdot\boldsymbol{v} = 0. \tag{A.3}$$

A.2 Equation of Motion

The conservation of momentum is written as

$$\frac{\mathrm{d}}{\mathrm{d}t}\int_{V(t)}\rho\boldsymbol{v}\mathrm{d}\boldsymbol{r}=\int_{V(t)}\rho\boldsymbol{f}\mathrm{d}\boldsymbol{r}+\int_{\Omega(t)}S\cdot\boldsymbol{n}\mathrm{d}\Omega, \tag{A.4}$$

where $\boldsymbol{f}$ is the force per unit mass and S is the stress tensor [1]. Using Gauss' theorem, we obtain

$$\rho\frac{\mathrm{D}}{\mathrm{D}t}\boldsymbol{v}=\rho\boldsymbol{f}+\nabla\cdot S. \tag{A.5}$$

Here we used the equation of continuity (A.3) and the relation (A.2).

A.3 Equation of Microrotation

From Eqs. (A.2) and (A.5), we have

$$\frac{\mathrm{d}}{\mathrm{d}t}\int_{V(t)}\rho(\boldsymbol{r}\times\boldsymbol{v})\mathrm{d}\boldsymbol{r} \tag{A.6}$$

$$=\int_{V(t)}[\partial_t(\boldsymbol{r}\times\rho\boldsymbol{v})+(\boldsymbol{v}\cdot\nabla)(\boldsymbol{r}\times\rho\boldsymbol{v})+(\boldsymbol{r}\times\rho\boldsymbol{v})(\nabla\cdot\boldsymbol{v})]\mathrm{d}\boldsymbol{r} \tag{A.7}$$

$$=\int_{V(t)}\boldsymbol{r}\times[\rho\mathrm{D}_t\boldsymbol{v}]\mathrm{d}\boldsymbol{r} \tag{A.8}$$

$$=\int_{V(t)}\boldsymbol{r}\times[\rho\boldsymbol{f}+\nabla\cdot S]\mathrm{d}\boldsymbol{r}. \tag{A.9}$$

On the other hand, the conservation of the angular momentum is expressed as

$$\frac{\mathrm{d}}{\mathrm{d}t}\int_{V(t)}\rho[\boldsymbol{l}+\boldsymbol{r}\times\boldsymbol{v}]\mathrm{d}\boldsymbol{r}=\int_{V(t)}\rho[\boldsymbol{r}\times\boldsymbol{f}]\mathrm{d}\boldsymbol{r}+\int_{\Omega(t)}[C\cdot\boldsymbol{n}+\boldsymbol{r}\times(S\cdot\boldsymbol{n})]\mathrm{d}\Omega \tag{A.10}$$

with the angular momentum of the microrotaion $\rho\boldsymbol{l}$ [2] and the couple stress C. [3]

[1] The component of the stress tenser S_{ij} is defined as the j component of the force acting on the plane perpendicular to the i direction. Therefore, the inner product of the tensor and the vector $S\cdot\boldsymbol{n}$ means $S_{ji}n_j$ and $(\nabla\cdot S)_i\equiv\partial_j S_{ji}$.

[2] $\rho\boldsymbol{l}\equiv nI\boldsymbol{\omega}$ in the system consists of identical spheres whose moments of inertia are I. Here, n and $\boldsymbol{\omega}$ are the number density and the angular velocity field, respectively.

[3] Here we do not consider the external torque, because such a term do not appear in the granular media.

When we use

$$\int_{V(t)} [\boldsymbol{r} \times (\nabla \cdot S)]_i \mathrm{d}\boldsymbol{r} \tag{A.11}$$

$$= \int_{V(t)} [\epsilon_{ijk} r_j \partial_m S_{mk}] \mathrm{d}\boldsymbol{r} \tag{A.12}$$

$$= \int_{V(t)} [\epsilon_{ijk} (\partial_m r_j S_{mk} - S_{jk})] \mathrm{d}\boldsymbol{r} \tag{A.13}$$

$$= \int_{V(t)} [\partial_m (\epsilon_{ijk} r_j S_{mk}) \mathrm{d}\boldsymbol{r} - \int_{V(t)} (\epsilon_{ijk} S_{jk}) \mathrm{d}\boldsymbol{r} \tag{A.14}$$

$$= \int_{\Omega(t)} [\boldsymbol{r} \times S \cdot \boldsymbol{n}] \mathrm{d}\Omega - \int_{V(t)} (\epsilon_{ijk} S_{jk}) \mathrm{d}\boldsymbol{r}, \tag{A.15}$$

we get

$$\int_{\Omega(t)} [\boldsymbol{r} \times S \cdot \boldsymbol{n}] \mathrm{d}\Omega = \int_{V(t)} [\boldsymbol{r} \times (\nabla \cdot S) + \boldsymbol{s}^{(a)}] \mathrm{d}\boldsymbol{r} \tag{A.16}$$

by using the vector defined from the asymmetric part of the stress tensor, $s_i^{(a)} \equiv \epsilon_{ijk} S_{jk}$. Thus Eq. (A.10) reads

$$\frac{\mathrm{d}}{\mathrm{d}t} \int_{V(t)} \rho [\boldsymbol{l} + \boldsymbol{r} \times \boldsymbol{v}] \mathrm{d}\boldsymbol{r} = \int_{V(t)} [\rho \boldsymbol{r} \times \boldsymbol{f} + \nabla \cdot C + \boldsymbol{r} \times (\nabla \cdot S) + \boldsymbol{s}^{(a)}] \mathrm{d}\boldsymbol{r}. \tag{A.17}$$

Considering Eq. (A.9), we obtain

$$\frac{\mathrm{d}}{\mathrm{d}t} \int_{V(t)} \rho \boldsymbol{l} \mathrm{d}\boldsymbol{r} = \int_{V(t)} [\nabla \cdot C + \boldsymbol{s}^{(a)}] \mathrm{d}\boldsymbol{r}. \tag{A.18}$$

Again from Eqs. (A.2) and (A.3), we have

$$\frac{\mathrm{d}}{\mathrm{d}t} \int_{V(t)} \rho \boldsymbol{l} \mathrm{d}\boldsymbol{r} = \int_{V(t)} [\partial_t \rho \boldsymbol{l} + \boldsymbol{v} \cdot \nabla \rho \boldsymbol{l} + \rho \boldsymbol{l} \nabla \cdot \boldsymbol{v}] \mathrm{d}\boldsymbol{r} \tag{A.19}$$

$$= \int_{V(t)} \rho [\partial_t + \boldsymbol{v} \cdot \nabla] \boldsymbol{l} \mathrm{d}\boldsymbol{r}. \tag{A.20}$$

From Eqs. (A.18) and (A.20), we finally obtain

$$\rho \frac{\mathrm{D}}{\mathrm{D}t} \boldsymbol{l} = \nabla \cdot C + \boldsymbol{s}^{(a)}. \tag{A.21}$$

Appendix B

A Soft Ball on the Floor

When a soft ball is in contact with the floor, the equation of motion for the overlap of the ball and the floor, z, is given by Eq. (4.4);

$$\ddot{z} + k_n z + \eta_n \dot{z} = g. \tag{B.1}$$

The solution of this equation is

$$z(t) = \exp\left(-\frac{1}{2}\eta_n t\right)\left[-\frac{g}{k_n}\cos(\Omega t) + B(v_0)\sin(\Omega t)\right] + \frac{g}{k_n}, \tag{B.2}$$

where

$$\Omega = \sqrt{k_n - \frac{\eta_n^2}{4}}, \tag{B.3}$$

and

$$B(v_0) = \frac{v_0 - g\eta_n/(2k_n)}{\Omega}. \tag{B.4}$$

Here we have assumed that the impact velocity is v_0. Note that $\eta_n \propto \sqrt{k_n}$ (see Eq. (4.1)) and thus $\Omega \propto \sqrt{k_n}$. The collision ends when $z(T_c) = 0$, and the restitution coefficient is determined by $|\dot{z}(T_c)/v_0|$.

When $v_0 \sim O(1) >> 1/\sqrt{k_n}$, the solution (B.2) is approximated as

$$z(t) = \exp\left(-\frac{1}{2}\eta_n t\right)\left[\frac{v_0}{\Omega}\sin(\Omega t)\right] + O\left(k_n^{-1}\right). \tag{B.5}$$

The leading order gives the constant restitution coefficient $e_w = \exp(-\eta_n \tau_w/2)$ with the constant duration of contact with the floor $\tau_w = \pi/\Omega$.

The critical impact velocity v_c below which the the ball stays in contact with the floor is determined by the condition $\dot{z}(T_c) = 0$, where T_c is the smallest positive solution of $z(T_c) = 0$. The constant e_w based on Eq. (B.5)

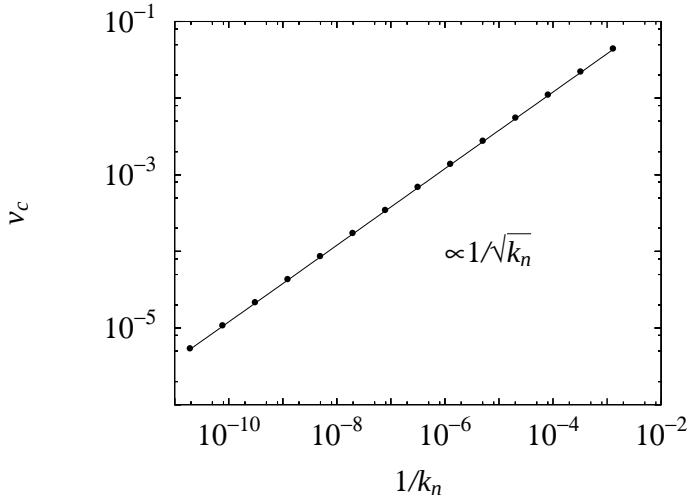

Figure B.1: The stiffness parameter k_n dependence of the critical impact velocity v_c below which the ball remains in contact with the floor. The filled circles are numerically obtained value, which agree with the solid line proportional to $1/\sqrt{k_n}$. The values of k_n and η_n are those used in Caper 4, which give $e_n = 0.7$.

indicates that v_c is not $O(1) >> 1/\sqrt{k_n}$. When $v_0 \sim O(1/\sqrt{k_n})$, all the terms in Eq. (B.2) become the same order ($O(1/k_n)$) and the condition $\dot{z}(T_c) = 0$ can be satisfied; namely, v_c should be $O(1/\sqrt{k_n})$. The numerically obtained k_n dependence of v_c are plotted in Fig. B.1, which shows $v_c \propto 1/\sqrt{k_n}$.

Bibliography

[1] H. M. Jaeger, S. R. Nagel, and R. P. Behringer. Granular solids, liquids, and gases. *Rev. Mod. Phys.*, Vol. 68, No. 4, p. 1259, October 1996.

[2] L. P. Kadanoff. Built upon sand: Theoretical ideas inspired by granular flows. *Rev. Mod. Phys.*, Vol. 71, No. 1, p. 435, 1999.

[3] P. G. de Gennes. Granular matter: a tentative view. *Rev. Mod. Phys.*, Vol. 71, p. S374, 1999.

[4] Ancey C. Dry granular flows down an inclined channel: Experimental investigations on the frictional-collisional regime. *Phys. Rev. E*, Vol. 65, p. 011304, 2001.

[5] P. K. Haff. Grain flow as a fluid-mechanical phenomenon. *J. Fluid Mech.*, Vol. 134, p. 401, 1983.

[6] J. T. Jenkins and S. B. Savage. A theory for the rapid flow of identical, smooth, nearly elastic, spherical particles. *J. Fluid Mech.*, Vol. 130, p. 187, 1983.

[7] C. S. Campbell. Rapid granular flows. *Ann. Rev. Fluid Mech.*, Vol. 22, p. 57, 1990.

[8] T. Pöschel and S. Luding, editors. *Granular Gases.* Springer-Verlag, Berlin, Germany, 2001.

[9] N. Sela and I. Goldhirsch. Hydrodynamic equations for rapid flows of smooth inelastic spheres, to Burnett order. *J. Fluid Mech.*, Vol. 361, p. 41, 1998.

[10] I. Goldhirsch. *in Modeling in Applied Sciences: A Kinetic Theory Approach.* Birkhäuser, Boston, 2000.

[11] J. Duran. *Sands, Powders, and grains: introduction to the physics of granular materials*. Springer, New York, 1997.

[12] M. Isobe. Simple and efficient algorithm for large scale molecular dynamics simulation in hard disk systems. *Int. J. Mod. Phys.*, Vol. C10, p. 1281, 1999.

[13] P. A. Cundall and O. D. L. Strack. A discrete numerical model for granular assemblies. *Geotechnique*, Vol. 29, p. 47, 1979.

[14] T. Pöschel. Granular material flowing down an inclined chute: a molecular dynamics simulation. *J. Phys. II (France)*, Vol. 3, p. 27, 1993.

[15] X. M. Zheng and J. M. Hill. Molecular dynamics simulation of granular flows: Slip along rough inclined planes. *Comput. Mech.*, 1998.

[16] D. Ertas, G. S. Grest, T. C. Halsey, D. Levine, and L. E. Silbert. Gravity-driven dense granular flows. *Europhys. Lett.*, Vol. 56, p. 214, 2001.

[17] L. E. Silbert, D. Ertas, G. S. Grest, T. C. Halsey, D. Levine, and S. J. Plimpton. Granular flow down an incline plane: Bagnold scaling and rheology. *Phys. Rev. E*, Vol. 64, p. 051302, 2001.

[18] L. E. Silbert, G. S. Grest, S. J. Plimpton, and D. Levine. Boundary effects and self-organization in dense granular flows. *Phys. Fluids*, Vol. 14, p. 2637, 2002.

[19] L. E. Silbert, D. Ertas, G. S. Grest, T. C. Halsey, and D. Levine. Analogies between granular jamming and the liquid-gas transition. *Phys. Rev. E*, Vol. 65, p. 051307, 2002.

[20] S. Yuu, T. Abe, T. Saitoh, and T. Umekage. Three-dimensional numerical simulation of the motion of particles discharging from a rectangular hopper using distinct element method and comparison with experimental data (effects of time steps and material properties. *Advanced Powder Technol.*, Vol. 6, p. 259, 1995.

[21] Y. Taguchi. Funryutai no Dourikigaku [in Japanese]. In H. Nishimori, H. Hayakawa, and Y. Taguchi, editors, *Physics of Granular Matter*, Vol. XI of *Selected Papers in Physics*, p. 30. The Physical Society of Japan, 1999.

[22] S. R. Kim and L. V. Woodcock. Kinetic theory of granular shear flow: constitutive relations for the hard sphere model. *J. Stat. Phys.*, Vol. 71, p. 174, 1993.

[23] H. Xu, M. Y. Louge, and J. T. Jenkins. Flow development of a sheared collisional granular flow. In Y. Kishino, editor, *Powders and Grains 2001*, p. 359, 2001.

[24] T. G. Drake. Granular flow: physical experiments and their implications for microstructual theories. *J. Fluid Mech.*, Vol. 225, p. 121, 1991.

[25] J. Cao, G. Ahmai, and M. Massoudi. Gravity granular flows of slightly frictional particles down an inclined bumpy chute. *J. Fluid Mech.*, Vol. 316, p. 197, 1996.

[26] E. Azanza, R. Chevoir, and P. Moucheront. Experimental study of collisional granular flows down an inclined plane. *J. Fluid Mech.*, Vol. 400, p. 199, 1999.

[27] A. C. Eringen. Simple microfluids. *Int. J. Engng. Sci.*, Vol. 2, p. 205, 1964.

[28] A. C. Eringen. Theory of micropolar fluids. *J. Math. Mech.*, Vol. 16, p. 1, 1966.

[29] G. Lukazewicz. *Micropolar Fluids: Theory and Applications*. Birkhäuser, Boston, 1999.

[30] H. Hayakawa. Slow viscous flows in micropolar fluids. *Phys. Rev. E*, Vol. 61, p. 5477, 2000.

[31] S. Horikawa, A. Nakahara, T. Nakayama, and M. Matsushita. Self-organized critical density waves of granular material flowing through a pipe. *J. Phys. Soc. Jpn.*, Vol. 64, p. 1870, 1995.

[32] M. Y. Louge. Computer simulations of rapid granular flows of spheres interacting with a flat, frictional boundary. *Phys. Fluids*, Vol. 6, p. 2253, 1994.

[33] F.-X. Riguidel, R. Jullien, G. H. Ristow, A. Hansen, and D. Bideau. Behavior of a sphere on a rough inclined plane. *J. Phys. I (France)*, Vol. 4, p. 261, 1994.

[34] G. H. Ristow, F. X. Ringuidel, and D. Bideau. Different characteristics of the motion of a single particle on a bumpy inclined plane. *J. Phys. I (France)*, Vol. 4, p. 1161, 1994.

[35] F. X. Ringuidel, A. Hansen, and D. Bideau. Gravity-driven motion of a particle on an inclined plane with controlled roughness. *Europhys. Lett.*, Vol. 28, p. 13, 1994.

[36] S. Dippel, G. G. Batrouni, and D. E. Wolf. Collision-induced friction in the motion of a single particle on a bumpy inclined line. *Phys. Rev. E*, Vol. 54, p. 6845, 1996.

[37] L. Samson, I. Ippolito, G. G. Batrouni, and J. Lemaitre. Diffusive properties of motion on a bumpy plane. *Euro. Phys. J. B*, Vol. 3, p. 377, 1998.

[38] L. Quartier, B. Andreotti, S. Douady, and A. Daerr. Dynamics of a grain on a sandpile model. *Phys. Rev. E*, Vol. 62, p. 8299, 2000.

[39] G. G. Batrouni, S. Dippel, and L. Samson. Stochastic model for the motion of a particle on an inclined plane and the onset of viscous friction. *Phys. Rev. E*, Vol. 53, p. 6469, 1996.

[40] S. Dippel, G. G. Batrouni, and D. E. Wolf. How transversal fluctuations affect the friction of a particle on a rough incline. *Phys. Rev. E*, Vol. 56, p. 3645, 1997.

[41] R. A. Bagnold. Experiments on a gravity-free dispersion of large solid spheres in a newtonian fluid under shear. *Proc. Roy. Soc. Lond. A*, Vol. 225, p. 49, 1954.

[42] S. Chapman and T. G. Cowling. *The mathematical theory of non-uniform gases.* Cambridge university press, Cambridge, 1970.

[43] I. Goldhirsch and G. Zanetti. Clustering instability in dissipative gases. *Phys. Rev. Lett.*, Vol. 70, p. 1619, 1993.

[44] S. McNamara and W. R. Young. Dynamics of a freely evolving, two-dimensional granular medium. *Phys. Rev. E*, Vol. 53, p. 5089, 1996.

[45] T. P. C. van Noije and M. H. Ernst. Cahn-hilliard theory for unstable granular fluids. *Phys. Rev. E*, Vol. 61, p. 1745, 2000.

[46] H. Nakanishi. Velocity distribution of inelastic granular gas in homogeneous cooling state. *cond-mat/0208477*, 2002.

[47] J. Bougie, S. J. Moon, J. B. Swift, and H. L. Swinney. Shocks in vertically oscillated granular layers. *Phys. Rev. E*, Vol. 66, p. 051301, 2002.

[48] C. S. Champbell. Boundary interactions for two-dimensional granular flows. part 1. flat boundaries, asymmetric stresses and couple stresses. *J. Fluid Mech.*, Vol. 247, p. 111, 1993.

[49] J. T. Jenkins and M. W. Richman. Kinetic theory for plane flows of a dense gas of identical, rough, inelastic, circular disks. *Phys. Fluids*, Vol. 28, p. 3485, 1985.

[50] C. K. K. Lun and S. B. Savage. A simple kinetic-theory for granular flow of rough, inelastic, spherical-particles. *J. Appl. Mech.*, Vol. 54, p. 47, 1987.

[51] C. K. K. Lun. Kinetic theory for granular flow of dense, slightly inelastic, slightly rough spheres. *J. Fluid Mech.*, Vol. 233, p. 539, 1991.

[52] K. Kanatani. *Funryutai no ryudo no kiso riron* [in japanese]. *Trans. Jpn. Soc. Mech. Eng. B*, Vol. 45, pp. 507,515, 1979.

[53] J. Kano, A. Shimosaka, , and J. Hidaka. *ryudo ryushigun no kousei kankei ni kansuru ichi kousatsu* [in Japanese]. *J. Soc. Powder Technol. Jpn.*, Vol. 33, p. 95, 1996.

[54] T. G. Drake. Structual features in granular flows. *J. Geophys. Res.*, Vol. 95, p. 8681, 1990.

[55] M. A. Hopkins and M. Y. Louge. Inelastic microstructure in rapid granular flows of smooth disks. *Phys. Fluids A*, Vol. 3, p. 47, 1991.

[56] O. Moriyama, N. Kuroiwa, M. Matsushita, and H. Hayakawa. 4/3 law of granular particles flowing through a vertical pipe. *Phys. Rev. E*, Vol. 80, p. 2833, 1998.

[57] J.-L. Aider, N. Sommier, T. Raafat, and J.-P. Hulin:. Experimental study of a granular flow in a vertical pipe: A spatiotemporal analysis. *Phys. Rev. E*, Vol. 59, p. 778, 1999.

[58] J. Lee and M. Leibig. Density waves in granular flow: a kinetic wave approach. *J. Phys. I France*, Vol. 4, p. 507, 1994.

[59] J. Lee. Density waves in the flows of granular media. *Phys. Rev. E*, Vol. 49, p. 281, 1994.

[60] T. Pöschel. Recurrent clogging and density waves in granular material flowing through a narrow pipe. *J. Phys. I France*, Vol. 4, p. 499, 1994.

[61] S. N. Prasad, D. Pal, and M. J. M. Römkens. Wave formation on a shallow layer of flowing grains. *J. Fluid Mech.*, Vol. 413, p. 89, 2000.

[62] M. Y. Louge and S. C. Keast. On dense granular flows down flat frictional inclines. *Phys. Fluids*, Vol. 13, p. 1213, 2001.

[63] T. S. Komatsu, S. Inagaki, N. Nakagawa, and S. Nasuno. Creep motion in granular pile exhibiting steady surface flow. *Phys. Rev. Lett.*, Vol. 86, p. 1757, 2001.

[64] A. V. Orpe and D. V. Khakhar. Scaling relations for granular flow in quasi-two-dimensional rotating cylinders. *Phys. Rev. E*, Vol. 64, p. 031302, 2001.

[65] D. Bonamy, F. Daviaud, L. Laurent, M. Bonetti, and J. P. Bouchaud. Multiscale clustering in granular surface flows. *Phys. Rev. Lett.*, Vol. 89, p. 034301, 2002.

[66] S. B. Savage. Gravity flow of cohesionless granular materials in chutes and channels. *J. Fluid Mech.*, Vol. 92, p. 53, 1979.

[67] L. E. Silbert, J. W. Landry, and G. S. Grest. Granular flow down a rough inclined plane: transition between thin and thick piles. *cond-mat/0206188*, 2002.

[68] P. C. Johnson and R. Jackson. Frictional-collisional constitutive relations for granular materials, with application to plane shearing. *J. Fluid Mech.*, Vol. 176, p. 67, 1987.

[69] P. Mills, D. Loggia, and M. Tixier. Model for a stationary dense granular flow along an inclined wall. *Europhys. Lett.*, Vol. 45, p. 733, 1999.

[70] B. Andreotti and S. Douady. Selection of velocity profile and flow depth in granular flows. *Phys. Rev. Lett.*, Vol. 63, p. 0131305, 2001.

[71] S. Douady, B. Andreotti, and A. Daerr. On granular surface flow equations. *Eur. Phys. J. B*, Vol. 11, p. 131, 1999.

[72] A. Aradian, E. Raphael, and P.-G. de Gennes. Surface flows of granular materials: A short introduction to some recent models. *C. R. Phys.*, Vol. 3, p. 187, 2002.

[73] S. Douady, B. Andreotti, A. Daerr, and P. Clade. The four fronts and the two avalanches. In Y. Kishino, editor, *Powders and Grains 2001*, p. 443, 2001.

[74] D. Ertas and T. C. Halsey. Granular gravitational collapse and chute flow. *cond-mat/020646*, 2002.

[75] O. Pouliquen. Scaling laws in granular flows down rough inclined planes. *Phys. Fluids*, Vol. 11, p. 542, 1999.

[76] A. Lemaitre. Origin of a repose angle: Kinetics of rearrangement for granular materials. *Phys. Rev. Lett.*, Vol. 89, p. 06303, 2002.

[77] L. Bocquet, J. Errami, and T. C. Lubensky. Hydrodynamic model for a dynamical jammed-to-flowing transition in gravity driven granular media. *Phys. Rev. Lett.*, Vol. 89, p. 184301, 2002.

[78] The Society of Powder Technology Japan, editor. *Funtai Simulation Nyumon (Introduction to Simulations of Granular Materials) [in Japanese]*. Sangyo Tosho, Tokyo, 1998.

[79] H. Hayakawa and S. Nasuno. *Funtai no Butsuri*, chapter 2. Gendai Butsurigaku Saizensen 1. Kyoritsu Shuppan, Tokyo, 2000.

[80] S. Luding. Granular materials under vibration: Simulations of rotating spheres. *Phys. Rev. E*, Vol. 52, p. 4442, 1995.

[81] C. Bizon, M. D. Shattuck, J. B. Swift, and H. L. Swinney. Transport coefficients for granular media from molecular dynamics simulations. *Phys. Rev. E*, Vol. 60, p. 4340, 1999.

[82] M. Isobe and H. Nakanishi. Phase changes in inelastic hard disk systems with a heat bath under the weak gravity for granular fluidization. *J. Phys. Soc. Jpn.*, Vol. 68, p. 2882, 1999.

[83] J. Schäfer, S. Dippel, and D. E. Wolf. Force schemes in simulations of granular materials. *J. Phys. I (France)*, Vol. 6, p. 5, 1996.

[84] H. Kuninaka and H. Hayakawa. The impact of two-dimensional elastic disk. *J. Phys. Soc. Jpn.*, Vol. 70, p. 2220, 2001.

[85] M. Y. Louge and M. E. Adams. Anomalous behavior of normal kinematic restitution in the oblique impacts of a hard sphere on an elastoplastic plate. *Phys. Rev. E*, Vol. 65, p. 021303, 2002.

[86] L. D. Landau and E. M. Lifshitz. *Theory of Elasticity (3rd edition).* Pergamon Press, 1986.

[87] Kokuritsu tenmondai, editor. *Rika Nenpyo [in Japanese]*, Vol. 63. Maruzen, 1990.

[88] B. Bernu and R. Mazighi. One-dimensional bounce of inelastically colliding marbles on a wall. *J. Phys. A: Math. Gen.*, Vol. 23, p. 5745, 1990.

[89] S. McNamara and W. R. Young. Inelastic collapse and clumping in a one-dimensional granular medium. *Phys. Fluids A*, Vol. 4, p. 496, 1992.

[90] S. McNamara and W. R. Young. Inelastic collapse in two dimensions. *Phys. Rev. E*, Vol. 50, p. R28, 1994.

[91] N. Schörghofer and T. Zhou. Inelastic collapse of rotating spheres. *Phys. Rev. E*, Vol. 54, p. 5511, 1996.

[92] M. Alam and C. M. Hrenya. Inelastic collapse in simple shear flow of granular medium. *Phys. Rev. E*, Vol. 63, p. 061308, 2001.

[93] P. Henrici. *Discrete Variable Methods in Ordinary Differential Equations.* Jhon Wiley & Sons, New York, 1962.

[94] F. Chevoir, M. Prochnow, J. T. Jenkins, and P. Mills. Dense granular flows down an inclined plane. In Y. Kishino, editor, *Powders and Grains 2001*, p. 373, 2001.

[95] H. Hayakawa. Note on a micropolar gas-kinetic theory. *cond-mat/0201231, to be published in the Proceedings of Traffic and Granular Flow 2001.*

[96] B. J. McCoy, S. I. Sandler, and J. S. Dahler. Transport properties of polyatomic fluids. iv. the kinetic theory of a dense gas of perfectly rough spheres. *J. Chem. Phys.*, Vol. 45, p. 3485, 1966.

[97] J. S. Dahler and M. Theodosopulu. The kinetic theory of dense polyatomic fluids. *Adv. Chem. Phys.*, Vol. 31, p. 155, 1975.

[98] F. Reif. *Berkeley physics course vol.5, Statistical Physics.* McGraw-Hill, New York, 1965.

[99] D. W. Condiff and J. S. Dahler. Fluid mechanical aspects of antisymmetric stress. *Phys. Fluids*, Vol. 7, p. 842, 1964.

[100] C. T. Veje, D. W. Howell, and R. P. Behringer. Kinematics of a two-dimensional granular couette experiment at the transition to shearing. *Phys. Rev. E*, Vol. 59, p. 739, 1999.

[101] D. M. Mueth, G. F. Debregeas, G. S. Karczmar, P. J. Eng, S. R. Nagel, and H. M. Jaeger. Signatures of granular microstructure in dense shear flows. *Nature*, Vol. 406, p. 385, 2000.

[102] M. Lätzel, S. Luding, and H. J. Herrmann. Macroscopic material properties from quasi-static, microscopic simulations of a two-dimensional shear-cell. *Gran. Matt.*, Vol. 2, p. 123, 2000.

[103] J. P. Bardet and I. Vardoulakis. The asymmetry of stress in granular media. *Solids Struct.*, Vol. 38, p. 353, 2001.

[104] H. B. Mühlhaus and P. Hornby. Energy and averages in the mechanics of granular materials. *Tectonophysics*, Vol. 335, p. 63, 2001.

[105] N. Mitarai and H. Nakanishi. Stability analysis of optimal velocity model for traffic and granular flow under open boundary condition. *J. Phys. Soc. Jpn.*, Vol. 68, p. 2475, 1999.

[106] N. Mitarai and H. Nakanishi. Spatiotemporal structure of traffic flow in a system with an open boundary. *Phys. Rev. Lett.*, Vol. 85, p. 1766, 2000.

[107] N. Mitarai and H. Nakanishi. Convective instability and structure formation in traffic flow. *J. Phys. Soc. Jpn*, Vol. 69, p. 3752, 2000.

[108] Y. C. Fung. *A First Course in Continuum Mechanics, Second Edition*, chapter 10. Prentice-Hall, New Jersey, U.S.A., 1977.

Publication list

March 13, 2003

1. Namiko Mitarai and Hiizu Nakanishi
   "Hard-sphere limit of soft-sphere model for granular materials: Stiffness dependence of steady granular flow"
   Phys. Rev. E **67**, art. no. 021301 (2003).
   (e-print: cond-mat/0210630)

2. Namiko Mitarai, Hisao Hayakawa, and Hiizu Nakanishi
   "Collisional Granular Flow as a Micropolar Fluid"
   Phys. Rev. Lett. **88**, art. no. 174301 (2002).
   (e-print: cond-mat/0108192)

3. Namiko Mitarai and Hiizu Nakanishi
   "Instability of Dilute Granular Flows on Rough Slope"
   J. Phys. Soc. Jpn. **70**, pp. 2809-2812 (2001).
   (e-print: cond-mat/0104571)

4. Namiko Mitarai and Hiizu Nakanishi
   "Convective Instability and Structure Formation in Traffic Flow"
   J. Phys. Soc. Jpn. **69**, pp. 3752-3761 (2000).

5. Namiko Mitarai and Hiizu Nakanishi
   "Spatiotemporal structure of traffic flow in a system with an open boundary"
   Phys. Rev. Lett. **85**, pp. 1766-1769 (2000).
   (e-print: cond-mat/0004294)

6. Namiko Mitarai and Hiizu Nakanishi
   "Stability Analysis of Optimal Velocity Model for Traffic and Granular Flow under Open Boundary Condition"
   J. Phys. Soc. Jpn. **68**, pp. 2475-2478 (1999).
   (e-print: cond-mat/9905315)